

Original Article

Cite this article: Dilek Y and Tang L (2021) Magmatic record of the Mesozoic geology of Hainan Island and its implications for the Mesozoic tectonomagmatic evolution of SE China: effects of slab geometry and dynamics in continental tectonics. *Geological Magazine* 158: 118–142. <https://doi.org/10.1017/S0016756820001211>

Received: 20 July 2018
Revised: 6 October 2020
Accepted: 9 October 2020
First published online: 10 December 2020

Keywords:

Mesozoic tectonics; flat subduction; chemical geodynamics; Hainan Island; slab-controlled push-over vs pull-away tectonics; extensional tectonics and magmatism; Jurassic–Cretaceous SE China; Triassic shortening; Yangtze Block

Author for correspondence: Yildirim Dilek,
Email: dileky@miamioh.edu

Magmatic record of the Mesozoic geology of Hainan Island and its implications for the Mesozoic tectonomagmatic evolution of SE China: effects of slab geometry and dynamics in continental tectonics

Yildirim Dilek¹  and Limei Tang²

¹Department of Geology & Environmental Earth Science, Miami University, Oxford, OH 45056, USA and ²Key Laboratory of Submarine Geosciences, Second Institute of Oceanography, MNR, Hangzhou 310012, China

Abstract

Our field-based geochemical studies of the Triassic, Jurassic and Cretaceous granitoids on Hainan Island indicate that their magmas had different geochemical affinities, changing from alkaline in the Triassic through ocean island basalt (OIB) in the Jurassic, to calc-alkaline in the Cretaceous. We show that these changes in the geochemical affinities of the Mesozoic granitoids on Hainan and in SE China reflect different melt sources and melt evolution patterns through time. Our new geodynamic model suggests that: (1) Triassic geology was controlled by flat-slab subduction of the palaeo-Pacific plate beneath SE China. This slab dynamics resulted in strong coupling between the lower and upper plates, causing *push-over tectonics* and contractional deformation in SE China. Flat subduction-induced edge flow and aesthenospheric uprising led to the production of high-K granites, syenites and mafic rocks. (2) Slab foundering, accelerated subduction rates and subduction hinge retreat in the Early Jurassic caused rapid rollback of the downgoing slab. Strong decoupling of the upper and lower plates resulted in *pull-away tectonics*, producing extensional deformation in SE China. Decompression melting of the upwelling aesthenosphere produced OIB-type melts, which interacted with the subcontinental lithospheric mantle (SCLM) to form A- and I-type granitoids. (3) Segmentation of the palaeo-Pacific plate in the Early Cretaceous resulted in steeply dipping slabs and their faster rollback, facilitating lithospheric-scale extension and oceanward migration of calc-alkaline magmatism. This extensional deformation played a significant role in the formation of metamorphic core complexes, widespread crustal melting and development of a Basin and Range-type tectonics and landscape evolution in SE China.

1. Introduction

The Mesozoic–Cenozoic geology of SE China is characterized by extensive magmatism, contractional and extensional deformation related, large-scale structures (i.e. SE China fold-and-thrust belt, Xuefeng Uplift, East China Rift System, Yangtze Fold Zone) and strike-slip fault systems (Figs 1, 2). Southeast China consists of two continental blocks, Yangtze and Cathaysia, making up the South China Block, which constitutes a significant component of the tectonic mosaic of SE Asia. The South China Block is separated from the North China Block to the north by the Qinling–Dabie–Sulu orogenic belt, from the Songpan Ganzi terrane to the NW by the Longmenshan fault system, from the Indochina Block to the SW by the Ailaoshan – Song Ma suture zone, and from the Luzon island arc (part of the Philippine Sea plate) to the E-SE by an active collision zone, exposed on the island of Taiwan (Fig. 1).

Although the tectonic boundaries of the South China Block with the surrounding continental blocks are well defined both geologically and geophysically, our understanding of the internal, lithospheric-scale architecture of this major cratonic block is still evolving as more data become available. Controversies and different interpretations exist, for example, as to what geological phenomena caused significant shortening of the crust in SE China during the Triassic, and what the driving forces were for the generally NW–SE-oriented extensional deformation, particularly within Cathaysia, during the Middle Jurassic through Cretaceous. Similarly, the heat and melt sources of extensive continental magmatism in SE China during the Triassic, Jurassic and Cretaceous periods and the potential drivers of these discrete magmatic episodes with different geochemical signatures remain controversial despite a vast amount of extant geochemical, geochronological and petrological data.

A major shortening event in the Triassic produced a NE-trending, ~1000 km wide fold-and-thrust belt (Fig. 1), which shows NW-younging ages for contractional structures (Faure *et al.* 2016;

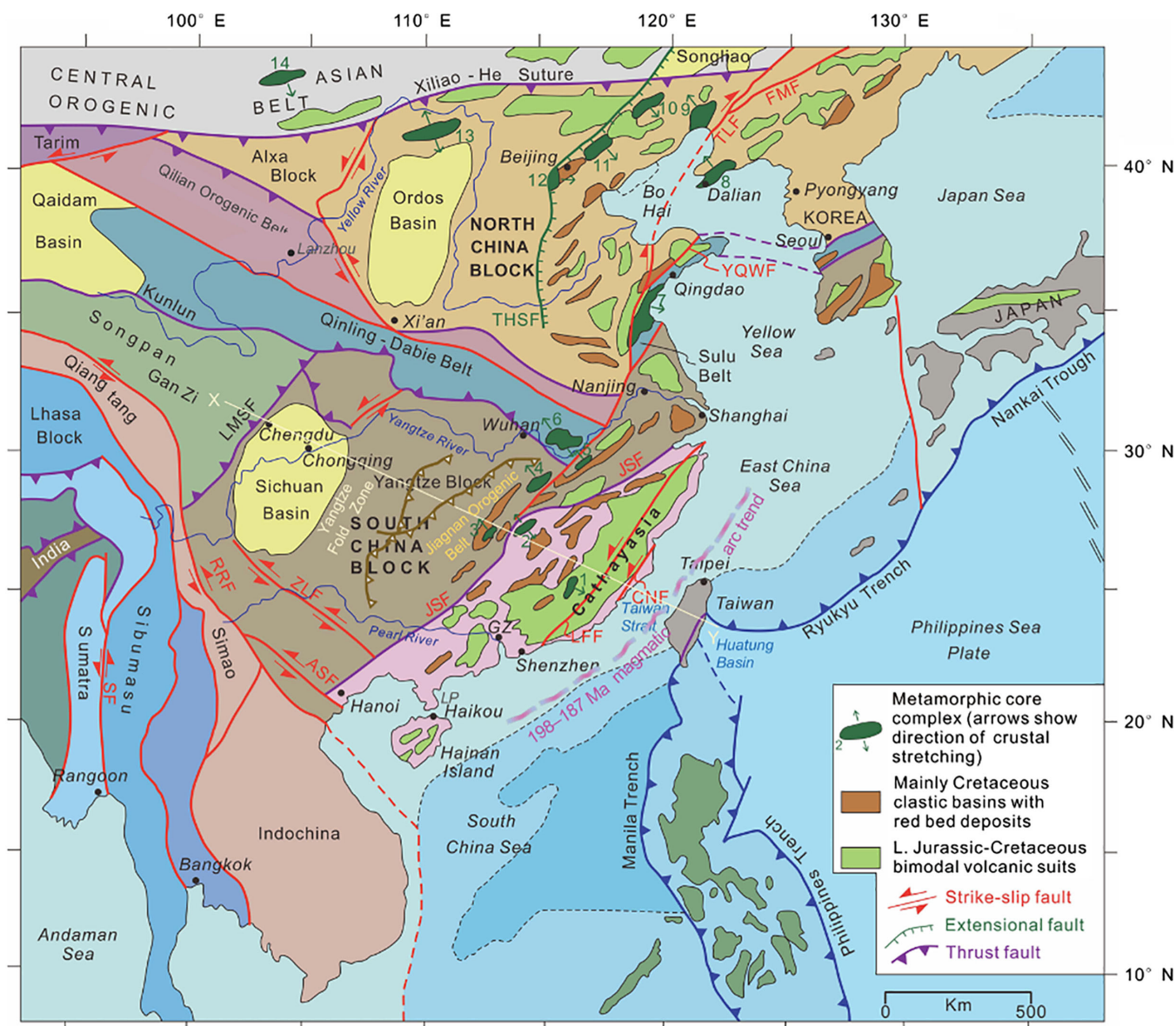


Fig 1. Simplified tectonic map of eastern and central China, Indochina and the western Pacific realm, showing the distribution of major continental blocks, suture zones, fault systems and modern trenches. Also shown, related to the topic of this paper, are latest Jurassic – Early Cretaceous metamorphic core complexes, Cretaceous clastic basins with red bed deposits, and Late Jurassic – Cretaceous bimodal volcanic sequences in eastern China. Metamorphic core complexes (listed from south to north): 1. Zhuguang–Nanxiong (102–96 Ma); 2. Wugongshan (131 Ma); 3. Yuechengling (140–120 Ma and 100–85 Ma); 4. Lushan (126 Ma); 5. Hongzhen (135–125 Ma); 6. North Dabieshan (125 Ma); 7. Wulian (135–122 Ma); 8. Liaoning (125 Ma); 9. Yiwulushan (126 Ma); 10. Kalajin (120 Ma); 11. Yunmengshan (126 Ma); 12. Xishan (132 Ma); 13. Hohhot (125–121 Ma); 14. Yagan–Onch Hayrhan Fault (126 Ma). Abbreviations for the major fault systems: ASF – Aliaoshan Fault; CNF – Changle–Nanao Fault; FMF – Fushun–Mishan Fault; LFF – Lishui–Haifang Fault; LMSF – Longmenshan Fault; NJF – Nenjiang Fault; RRF – Red River Fault; SF – Sagaing Fault; THSF – Taihangshan Fault; YQWF – Yantai–Qingdao Wulian Fault; ZLF – Ziyun–Luodian Fault. LP – Leizhou (Liuchow) Peninsula. Data are from Faure *et al.* (1996), Wang *et al.* (2001), Lin & Wang (2006), Hall (2012), Ni *et al.* (2013), GW Zhang *et al.* (2013), Li & Li (2015), CH Xu *et al.* (2017) and Chu *et al.* (2019).

Li *et al.* 2017, 2018, and references therein). Interpretations for the cause of this deformation include: (1) far-field stress effects of the collisions between the North and South China blocks in the Early Palaeozoic (Faure *et al.* 2008) or in the Late Triassic (Meng & Zhang, 1999); (2) the collision of the Indochina and South China blocks in the Early to Middle Triassic (Zhang & Cai, 2009; Xu *et al.* 2011; Wang *et al.* 2013; Faure *et al.* 2014; Shu *et al.* 2015; Qiu *et al.* 2017); and (3) flat subduction along the active continental margin of East Asia (Zhou *et al.* 2006; Li & Li, 2007; JH Li *et al.* 2018; Tao *et al.* 2019).

Extensional tectonic and magmatic features in SE China include normal fault systems, metamorphic core complexes, and volcanic–

plutonic belts with diverse compositions and geochemical affinities (Figs 1, 2; LS Shu *et al.* 2009; Wang & Shu, 2012; JH Li *et al.* 2014; J Li *et al.* 2016; Wei *et al.* 2018). The main interpretations and models for the origin of these magmatic suites and the extensional fault systems include: (1) post-collisional collapse of thick continental crust (Zhou *et al.* 2006; Li & Li, 2007); (2) large-scale asthenospheric upwelling associated with the break-up of Gondwana ~190 Ma, leading to lithospheric thinning and magmatism between ~180 and 80 Ma (Wilde *et al.* 2003; Wang *et al.* 2017); (3) an extended continental arc origin (e.g. Zhou & Li, 2000); and (4) rollback of the subducting palaeo-Pacific plate and

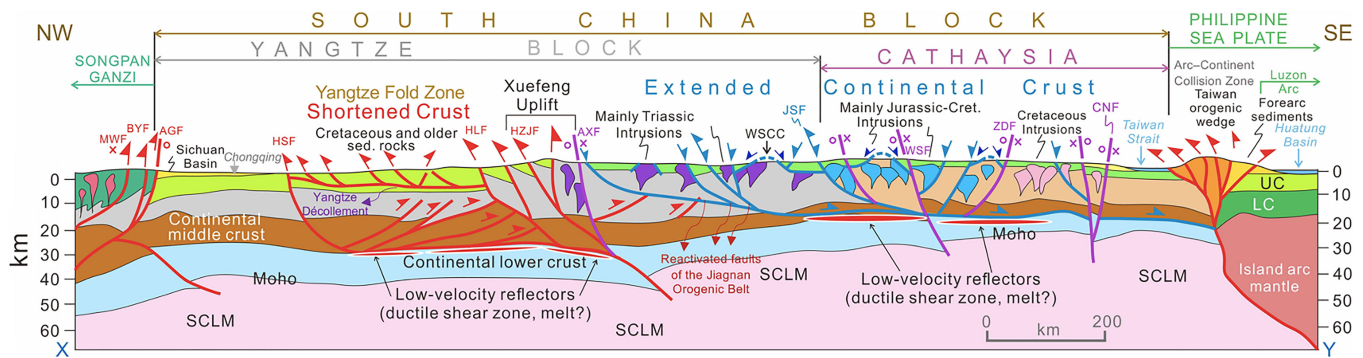


Fig 2. WNW-ESE-oriented lithospheric-scale tectonic cross-section, depicting the main modes of crustal and mantle deformation structures across the South China Block, extending into the Songpan Ganzi terrane in the NW and to the modern arc-continent collision zone in Taiwan and the Philippine Sea Plate in the SE. The Xuefeng Uplift Zone separates the folded and thrust-faulted Cretaceous and older sedimentary rocks of the Yangtze block (*Shortened Crust*) in the west from the *Extended Crust* of the Yangtze and Cathaysia blocks in the east. Geometries and locations of the main fault systems are based on seismically determined profile by Zhang *et al.* (2013). Other data are from XH Li (2000), Li & van der Hilst (2010), Wang & Shu (2012), Li *et al.* (2016), CH Xu *et al.* (2017), Zhang *et al.* (2017) and JH Li *et al.* (2018). Abbreviations for the major fault systems: AGF = Anxian-Guanxian Fault; AXF = Anhua-Xupu Fault; BYF = Beichuan-Yingxiu Fault; CNF = Changle-Nanao Fault; GJF = Ganjiang Fault; HLF = Hefeng-Laifeng Fault; HSF = Huayingshan Fault; HZJF = Huayuan-Zhangjiatie Fault; JSF = Jiangshan-Shaoxing Fault; LLF = Lishui-Faifang Fault; MWF = Maowan Fault; WWSF = Wuchuan-Sihui Fault; ZDF = Zhenghe-Dapu Fault. Other abbreviations: LC = lower continental crust; SCLM = subcontinental lithospheric mantle; UC = upper continental crust; WSCC = Wugongshan core complex (131 Ma). Note that some of the E-dipping extensional normal faults in the eastern Yangtze Block are reactivated W-directed Triassic (?) thrust faults. Notice the significantly thinned nature of the lithosphere, particularly the middle to lower crust, in eastern Yangtze and Cathaysia blocks, and the existence of low-velocity reflectors (representing ductile shear zones and/or melt lenses) near the top of the lower crust in Cathaysia.

associated extensional deformation and magmatism in the continental upper plate (Li *et al.* 2014, and references therein). The post-orogenic collapse models are problematic because: (a) granitic plutons and their volcanic counterparts in E-SE China are much more extensive in their areal coverage beyond the collision zones (i.e. Qinling-Dabie, Sulu, Ailaoshan and Jiang Saho sutures and fault zones), and these plutonic-volcanic rocks are spatially and temporally associated with extensional tectonic features (see, for example, Shu *et al.* (2009) and Wei *et al.* (2018) for Jurassic, and Yang *et al.* (2011), Zhao *et al.* (2019) and C Wang *et al.* (2017) for Cretaceous magmatic suites and related extensional tectonics); (b) their emplacement times are at least ~60–80 Ma after the collisional events, which represents a very large time window in comparison to an average timespan for the initiation of post-collisional magmatism in other Mesozoic and Cenozoic orogenic belts (for some examples, see Dilek & Moores, 1999; Dilek & Whitney, 2000; Dilek, 2006; Dilek *et al.* 2010; Jamali *et al.* 2010); and (c) there is no viable explanation for the heat source to drive the lithospheric-scale magmatism. Significant variations in the geochemistry and melt origin of the plutonic and volcanic rocks do not support the second and third models above. The slab rollback model is still debatable because of the perceived problems with the timing of the onset of the palaeo-Pacific plate subduction beneath the continent, the nature of the slab dynamics (flat vs high-angle) and the apparent absence of a Jurassic-Cretaceous continental arc system in mainland SE China.

In this study, we investigate the Mesozoic structural architecture and magmatic record of Hainan Island in the South China Block, and the geochemical characteristics and melt evolution of its Triassic through Cretaceous granitoids. We show that the Mesozoic granitoids in Hainan display characteristic trends and patterns as a result of time-progressive evolution of their mantle melt sources and melt development through time that are highly similar to those of their counterparts in mainland SE China. Hence, we consider Hainan Island a microcosm of the Mesozoic geology of SE China. The Mesozoic Hainan granitoids provide a unique opportunity to evaluate the spatial and temporal relationships between magmatism and the regional tectonics. In the first part of the paper, we discuss the crustal architecture and geology

of Hainan, specifically the Mesozoic granitoids and the spatially associated intrusive rocks. Next, we present our geochemical and isotopic data on the Mesozoic granitoids on Hainan in comparison to the available data from coeval and similar granitoids in SE China. We then discuss the structural architecture and magmatic make-up of Mesozoic SE China in order to evaluate the nature of the spatial and temporal relationships between the regional tectonics and magmatism through time. The following section on the crustal and mantle structure beneath modern SE China helps us better understand the extreme heterogeneity in the crustal make-up of the South China Block that was reworked significantly during the Mesozoic. This heterogeneous continental crust in SE China strongly influenced the melt evolution of the Cretaceous granitoids and their volcanic counterparts. In the last part of the paper we present our new geodynamic model and propose that a slab-driven tectonic mode switch (Lister & Foster, 2009; Schellart *et al.* 2010) from *push-over* geodynamics in the Triassic–Early Jurassic to *pull-away* geodynamics in the later Jurassic–Cretaceous along the active margin of East Asia produced the contrasting tectonic regimes and styles in Mesozoic SE China. Our model differs from other existing tectonic switch models suggesting various external causes, and shows, instead, that changes in subducting slab widths, subduction velocities and the degree of coupling–decoupling between the lower and upper plates played a major role in driving tectonic mode switches during the Mesozoic evolution of SE China. We propose the late Cretaceous–Eocene tectonics of the Western US Cordillera as an analogue for the Mesozoic tectonics of SE China. We present this geodynamic model as a working hypothesis, which should be tested by future integrated studies in SE China.

2. Review of the regional geology of SE China

The regional geology of the South China Block displays two major suture zones along a NW–SE-oriented, lithospheric-scale tectonic profile (Fig. 2) that attest to its eastward growth via collisional events through time. These events are the Neoproterozoic amalgamation of the Yangtze and Cathaysia blocks (Charvet *et al.* 1996; Faure *et al.* 2009; ZX Li *et al.* 2010; Wang *et al.* 2012; Shu *et al.* 2014), and the

6.5 Ma collision of the Luzon volcanic arc of the Philippine Sea plate with the SE China Block (Byrne *et al.* 2011; Van Avendonk *et al.* 2016; Chen *et al.* 2017; Malavieille *et al.* 2020). In the opposite, NE–SW direction, the South China Block also underwent a series of collisional orogenic events as it sutured with the North China Block to the NE in the Late Triassic (Meng & Zhang, 1999) or perhaps earlier in the Palaeozoic (Faure *et al.* 2008), and with Indochina to the SW in the Early to Middle Triassic (Qiu *et al.* 2017). Here, we consider the lithospheric-scale structures of the South China Block between its NW and SE tectonic boundaries against the Songpan Ganzi terrane to the NW and the arc–continent collision zone in Taiwan to the SE, because we are interested in observing the crustal structure and magmatic record of SE China in the general direction of its major crustal growth (Figs 1, 2).

The NE–SW-oriented Jiang Shao fault zone (JSF) marks the main tectonic boundary between the Cathaysia and Yangtze continental blocks, and the nearly 150–200 km wide Jiagnan orogenic belt to the west of this fault zone (Figs 1, 2) represents a protracted period of multiple oceanic plate subduction and island arc collision events between the Yangtze and Cathaysia blocks throughout the Proterozoic, prior to their final suturing (Li *et al.* 2016, and references therein). The Proterozoic basement rocks within this Jiagnan orogenic belt include metamorphosed granitoid intrusions, mafic–ultramafic rock sequences, pelitic rocks and flysch deposits. The structural fabric in the orogenic belt is characterized by W–NW-vergent thrust faults, which were largely reactivated as low-angle normal faults in the Cretaceous (Li *et al.* 2016). Superimposed on the Jiagnan orogeny were the Triassic Indosinian orogeny and a Middle–Late Jurassic contractional event in the Yangtze Block. Interpretations of the mechanics and the causes of the Indosinian orogeny are diverse. It is mainly interpreted as an intracontinental event that produced NW-directed thrust faulting and folding, greenschist metamorphism and alkaline magmatism (Lin *et al.* 2008; Shu *et al.* 2009; Zhang & Cai, 2009; XB Xu *et al.* 2011; Chu *et al.* 2012), although alternative explanations invoking the continental collisions with the North China (Zhang & Cai, 2009) or Indochina blocks (Faure *et al.* 2014) have also been proposed. Carter & Cliff (2008) have argued that the Indosinian orogeny was a reactivation event caused by the accretion of the Shibumasu Block to Indochina further south in Vietnam, rather than a major mountain-building episode between the Indochina and South China blocks.

To the west of the Jiagnan orogenic belt is the Middle Triassic Xuefeng Uplift (Fig. 2), which is characterized by NW-directed shortening (Ma *et al.* 2019), NW–SE-oriented mineral lineation and NE–SW-trending folds. The timing of NW-directed thrusting, which involved the Proterozoic basement rocks and the Mesozoic metasedimentary rock sequences, was 243–226 Ma based on monazite dating of sheared micaschists (Chu *et al.* 2012).

A Middle–Late Jurassic contractional event was responsible for the development of a broad fold-and-thrust belt (*SE China Fold and Thrust Belt*; Fig. 3) and décollement surfaces at depth (Yang & Yu, 1994; Yan *et al.* 2003; Ding *et al.* 2007; Li *et al.* 2016). NE-trending folds were cross-cut by Late Jurassic granitic intrusions, indicating that folding and associated shortening must have developed in the Middle to Late Jurassic at the latest (Li *et al.* 2016). This event has been interpreted to have resulted from retroarc deformation above the palaeo-Pacific slab subducting beneath SE China (Li *et al.* 2016, and references therein).

The Yangtze Fold Zone (Fig. 1) to the west of the Xuefeng Uplift represents a long-wavelength crustal shortening zone, which is

characterized by thin-skinned, NW-vergent imbricate faulting and folding, underlain by a regional-scale décollement structure (*Main Yangtze Décollement*), which shows a down-dip flat–ramp–flat geometry to the SE on seismic reflection profiles (Fig. 2; JH Li *et al.* 2018). This décollement zone separates the highly deformed (shortened) upper crust from the underlying, weakly deformed middle crust, and accommodates strain decoupling between the two crustal levels (Li *et al.* 2016). The occurrence of low-velocity reflectors between the middle and lower continental crust beneath the Yangtze Fold Zone may point to the existence of ductile shear zone or thin melt lenses at ~30 km depth (Li & van der Hilst, 2010; Zhou *et al.* 2012; Zhang *et al.* 2017). The intense crustal shortening structures within the Yangtze Fold Zone diminish abruptly towards the Sichuan Basin to the west (Fig. 2). Thus, the continental crust of the South China Block to the west of the Anhua–Xupu Fault (AXF) underwent significant shortening at upper and middle crustal depths during the Mesozoic.

The SE Yangtze and the entire Cathaysia block contain Middle to Late Jurassic plutons and their volcanic counterparts (Early Yanshanian episode; 165–153 Ma; Fig. 3), and Cretaceous plutons, bimodal volcanic rocks and clastic sedimentary sequences (Late Yanshanian episode; 145–87 Ma; Figs 2, 3). Different interpretations for the origins of the Early and Late Yanshanian magmatic episodes also exist (see Li, 2000, for an overview). We discuss the Jurassic–Cretaceous magmatism and extensional deformation in detail in the later parts of the paper. However, two important geological features regarding the Jurassic and Cretaceous tectonics of SE China are important to point out here: (1) In the published literature, the lack of an exposed Jurassic magmatic arc complex in SE China has always been interpreted against the palaeo-Pacific plate subduction beneath SE China during the early Mesozoic. However, recent drilling in the NE part of the South China Sea has recovered core samples of high-Mg diorite and granite rocks with ages between 198 and 195 Ma, representing calc-alkaline arc suites (CH Xu *et al.* 2017). These Lower Jurassic calc-alkaline plutonic rocks have been interpreted to represent an Early Jurassic magmatic arc, which developed above a NW-dipping palaeo-Pacific oceanic slab (JH Li *et al.* 2018). The crystalline basement of the continental shelf in the northern South China Sea and the Taiwan Strait is thus likely to be composed of a subsided magmatic arc (Li *et al.* 2016; CH Xu *et al.* 2017). (2) Strike-slip faulting and related deformation appear to have become increasingly important in SE China from the Late Jurassic through the Cretaceous. Palaeo-stress investigations in and around the Huangshan Basin in Anhui Province (south of the Yangtze River) have shown that a right-lateral strike-slip regime with nearly E–W compression and N–S extension predominated in the region from the late Middle Jurassic through the Late Jurassic (X Xu *et al.* 2015). This stress regime was controlled by the subduction of the palaeo-Pacific slab beneath SE China. Then, a sinistral strike-slip regime with N–S compression and E–W extension predominated during the late Early Cretaceous, and it was induced by either the left-oblique subduction of the palaeo-Pacific slab or the oblique collision of the Philippine and SE China blocks in the Early Cretaceous (X Xu *et al.* 2015). This left-lateral strike-slip tectonics in SE China played a significant role in the development of transtensional sedimentary basins in E and SE China (Y Zhang *et al.* 2020, and references therein) and in the Korean Peninsula (DW Lee, 1999) during the Late Cretaceous–Early Palaeogene, and then in the initial opening of the proto-South China Sea in the Palaeocene–Eocene (CY Huang *et al.* 2019).

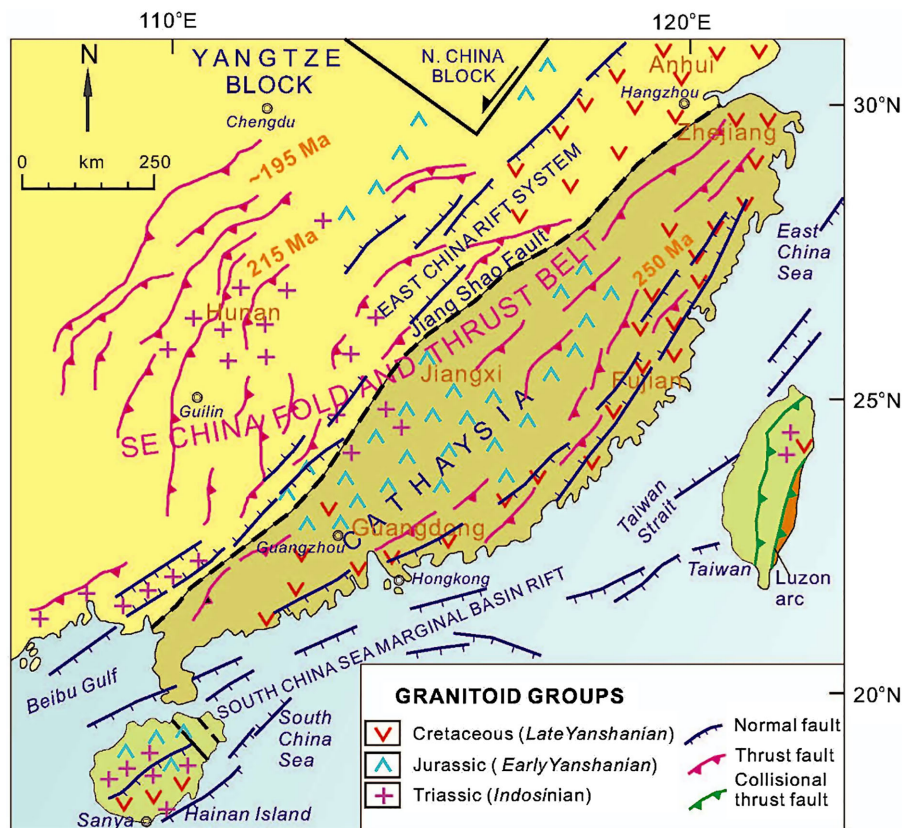


Fig 3. Simplified tectonic map of SE China, showing the distribution of major Mesozoic structural systems and granitoid groups. Data are from ZY Tian *et al.* (1992), Yang & Yu (1994), Li (2000), Xiao & He (2005), Jiang *et al.* (2006), Li *et al.* (2016), Wei *et al.* (2018) and Wang *et al.* (2020).

3. Hainan Island: geological microcosm of Mesozoic SE China

3.a. Crustal architecture and geology of Hainan

Hainan Island is located in the continental shelf of southern China and adjacent to the Indochina Block in the west (Fig. 1). It is also tectonically situated within the NE–SW-trending South China Marginal Basin Rift System, which extends into the Taiwan Strait in the NE (Fig. 3). The basement rocks on Hainan are covered peripherally by Quaternary alluvium, and by Quaternary intra-plate basaltic lava flows in the northern part of the island (Fig. 4; Tian *et al.* 2020). Similar lava fields continue to the north on the Leizhou (Liuchow) Peninsula in mainland China, making up the Leiqiong volcanic field. The structural fabric of Hainan Island is defined mainly by NE–SW-oriented, oblique normal fault systems, forming locally well-developed horst blocks (Fig. 4). The inverted Baisha basin, which is composed of Cretaceous sedimentary and volcanic rock sequences in the west-central part of the island with a highest peak of 1417 m a.s.l., represents one of these fault blocks.

The crystalline basement in Hainan consists of metamorphosed Mesoproterozoic magmatic, volcanic and clastic rocks that are exposed mainly in the W–SW and E parts of the island (Fig. 4). Amphibolite-facies gneissic granitoids, gneiss and metaclastic rocks of the 1430 Ma Baoban Complex represent a Mesoproterozoic continental rift sequence (Yao *et al.* 2017). Greenschist-facies metasedimentary and metavolcanic rocks of the 1439 ± 9 Ma Shilu Group constitute the upper crustal volcanic–sedimentary units of this rift sequence (Yao *et al.* 2017). The unconformably overlying 1200–1000 Ma metamorphosed quartz–sandstones of the Shihuiding Formation make up foreland deposits. Metamorphosed Lower Palaeozoic

sedimentary rocks are locally exposed both in the western and eastern parts of the island. These Mesoproterozoic crystalline and Lower Palaeozoic metasedimentary rocks are intruded by Permian (Wuzhishan), Triassic (Indosinian) and Jurassic–Cretaceous (Yanshanian) granitoids and are overlain by Lower and Upper Palaeozoic sedimentary–volcanic rock assemblages, and Upper Triassic clastic rocks (Fig. 4).

Permo–Carboniferous (333 Ma) metasedimentary and meta-volcanic rocks with mid-ocean-ridge basalt (MORB) affinities in the west-central part of the island represent a major episode of continental rifting in its Palaeozoic tectonic history (Li *et al.* 2002). Li *et al.* (2006) have demonstrated the occurrence of 267–262 Ma (Guadalupian), calc-alkaline metagranites (Wuzhishan orthogneiss) in east-central Hainan, which they have interpreted as the first major product of continental arc magmatism in SE China, developed above a NW-dipping subduction zone. These authors have also noted that this Permian, Andean-type arc magmatism was coeval with widespread crustal uplift along the coast of SE China that provided clastic sediments into terrestrial basins further inland. The timing of the Permian arc plutonism on Hainan is consistent with the findings of Zhang and co-workers in Anhui Province in SE China (FQ Zhang *et al.* 2020) where Guadalupian (270–264 Ma) tuff deposits within the Gufeng Formation (Permian carbonate platform of SE China) represent the initial products of subaerial volcanism and magmatic arc construction in SE China during the Late Palaeozoic.

3.b. Mesozoic granitoids and associated intrusive rocks on Hainan

In this study, we have distinguished two major (early–Middle Triassic and Cretaceous) igneous events in the geological record

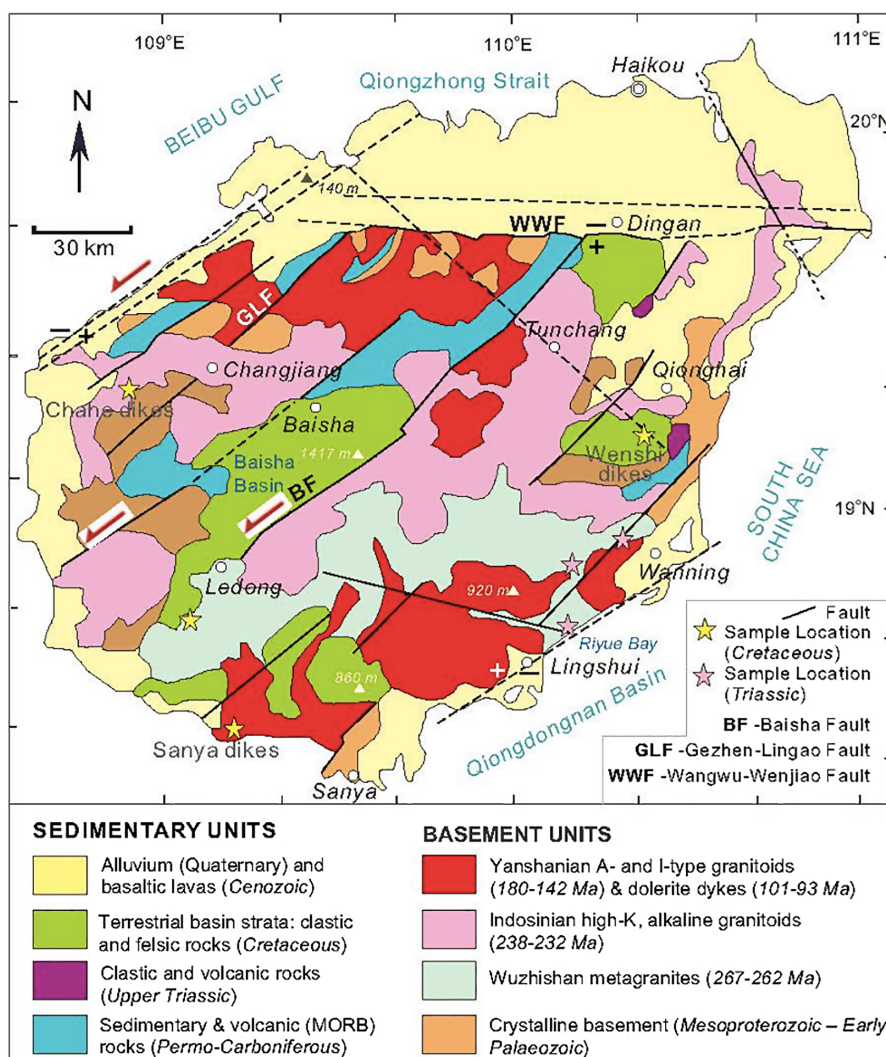


Fig 4. Geological map of Hainan Island, depicting the distribution of main fault systems, granitoid groups and sample locations for this study. Data are from XH Li *et al.* (2002), Ge, (2003), Li *et al.* (2006), Pedoja *et al.* (2008), Y Hu *et al.* (2016), D Xu *et al.* (2017), Yao *et al.* (2017), Tian *et al.* (2020) and this study.

of Hainan. Ge (2003) also reported the existence of Jurassic granitic intrusions (186 Ma) on Hainan Island. Triassic magmatic rocks include bimodal, high-K granites and hypabyssal dolerite, hornblende gabbro and syenite that are all alkaline to subalkaline in nature (Fig. 5). The distribution of these Triassic intrusions and their internal structural fabric are predominantly NE–SW oriented (Fig. 4). Contact relationships observed in the field suggest that the Xinglong granite intruded into the dolerite via magma stoping (Fig. 6a–c) and along extensional shear zones (Fig. 6d). These spatial relationships are best exposed below the river-bed dam in Dazhou Village, where irregular and anastomosing granite veins intrude the fine-grained dolerite and the larger outcrops of granite contain enclaves of dolerite. The dolerite rock is dark grey and displays an ophitic texture; it is composed mainly of plagioclase (70–60%), clinopyroxene (25–20%), amphibole (15–10%) and biotite (10–5%) (Fig. 7a). The Xinglong granite is red in both outcrop and hand sample and is coarse-grained. It is composed of plagioclase with microcline twinning (70–60%), quartz (25–20%), hornblende (10–5%) and biotite (10–5%) (Fig. 7b).

The Wanning gabbro is exposed on the north side of the Wanning reservoir near Wanning City (Fig. 4) and is intrusive into ~251–234 Ma mylonitic gneissic granites. It is coarse-grained and

composed predominantly of plagioclase (65–60%), hornblende (30–25%) and pyroxene (4–3%) (Fig. 7c). Accessory minerals include apatite, zircon and magnetite (2–1%). The Fenjiezhou syenite crops out on the small Fenjiezhou Island (or Boundary Island) in the Riyue Bay immediately to the SE of Hainan and is intrusive into Permo-Carboniferous metasedimentary rocks. It is composed of 75–70% feldspar, 10–5% albite, ~10% biotite and ~3% quartz.

Middle to Late Jurassic (180–142 Ma) granitoids (coexisting with minor dolerite, diorite and gabbro to syenite) and volcanic rock assemblages occur widely in NE–SW-trending belts in Hainan and SE China (Li *et al.* 2010; Zhou *et al.* 2006; Li & Li, 2007). Jurassic granitoids have geochemical characteristics of I- and A-type granites, whereas the coeval syenites show incompatible trace-element patterns of ocean island basalt (OIB)-type melts (Li *et al.* 2010; Zhou *et al.* 2006). These Jurassic granite and syenite intrusions are spatially and temporally associated with alkaline basalts and bimodal (basalt–rhyolite) volcanic rocks (180–170 Ma).

Cretaceous magmatic rocks on Hainan occur as mainly NE–SW-striking doleritic dyke swarms in the Proterozoic metamorphic basement units and in the Triassic granitoids (*Chahe dykes*), in Lower Cretaceous sandstone-conglomerate units (*Wenshi dykes*) and in the Jurassic–Cretaceous granite suites (*Sanya dykes*)

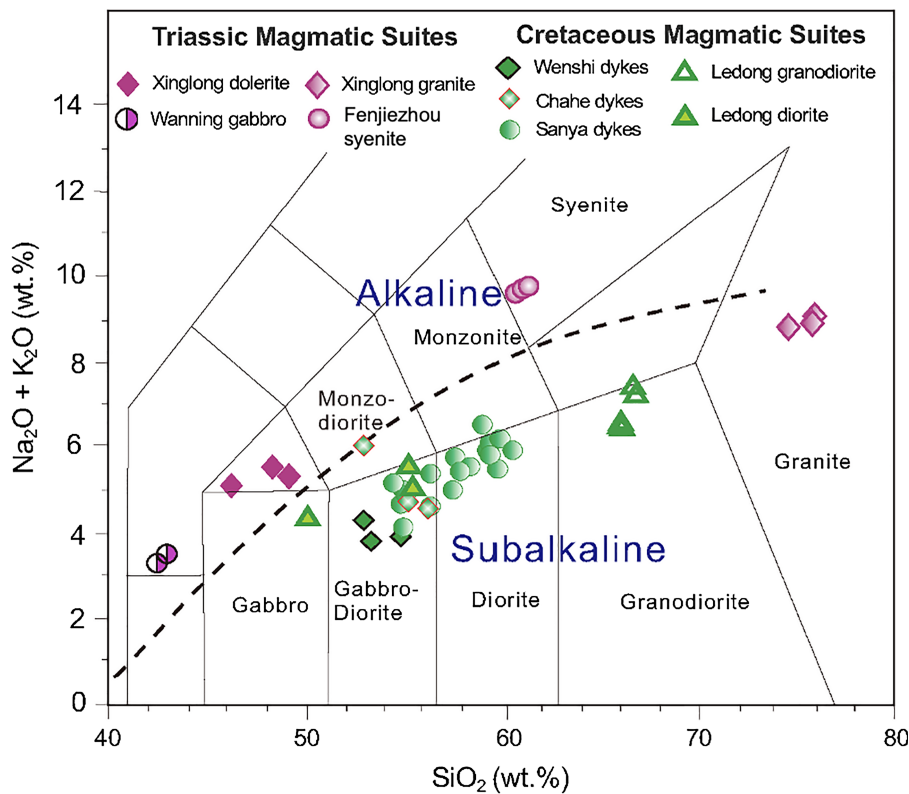


Fig 5. Total alkali vs SiO_2 diagram for the Triassic and Cretaceous intrusive rock suites on Hainan Island (this study). FJZ = Fenjiezhou syenite. Alkaline-subalkaline boundary is from Le Bas *et al.* (1986).

(Fig. 8). These dykes were intruded along NE–SW-oriented fault systems. Also part of the Cretaceous magmatic series is the Ledong diorite–granodiorite suite in the SW part of Hainan. Diorite occurs as enclaves within the granodiorite. The Chahe dykes occur in the west-central part of Hainan near the city of Changjiang, the Wenshi dykes occur in the east-central part near Wenshi Town in Qionghai City, and the Sanya dykes crop out along the Sanya City Highway in southern Hainan, west of the city of Sanya (Fig. 4). All dyke rocks are composed of dolerite with a diabasic texture and consist of plagioclase, pyroxene and hornblende with accessory minerals of apatite, zircon and magnetite (Fig. 7e–f).

3.c. Geochronology of Mesozoic intrusive rocks on Hainan

The hypabyssal dolerite and the Xinglong granite intrusions have U–Pb sensitive high-resolution microprobe (SHRIMP) zircon weighted mean $^{206}\text{Pb}/^{238}\text{U}$ concordia ages of 238 ± 2 Ma (MSDW = 0.69) and 234 ± 2 Ma (MSDW = 0.14), respectively (see Data Repository File #1 (in the Supplementary Material available online at <https://doi.org/10.1017/S0016756820001211>); Tang *et al.* 2013). SHRIMP zircon dating of the Wanning gabbro and Fenjiezhou syenite have weighted mean $^{206}\text{Pb}/^{238}\text{U}$ concordia ages of 240 ± 2 Ma and 231 ± 3.4 Ma, respectively (Tang *et al.* 2013). We interpret these ages as the timing of crystallization of the Wanning gabbro and hypabyssal dolerite, followed by the emplacement of the granite and syenite in the Middle to Late Triassic.

The dolerite dyke swarms display magmatic zircon ages between 101 ± 4 Ma and 93 ± 2 Ma (U–Pb SHRIMP dating), and inherited zircon ages of 238 ± 4 Ma and 237 ± 4 Ma (see Data Repository File #1 (in the Supplementary Material available online at <https://doi.org/10.1017/S0016756820001211>); Tang *et al.* 2013).

Magmatic zircons represent the timing of a widespread NE–SW-dyking event in a regional, NW–SE-oriented extensional stress regime. Inherited zircon ages are identical to the ages of the Triassic dolerite and granite intrusions on Hainan, indicating that the Cretaceous magmas came up through these earlier-formed intrusive series. The Ledong granodiorite zircons have weighted mean $^{206}\text{Pb}/^{238}\text{U}$ concordia ages of 101 ± 0.9 Ma (see Data Repository File #1 (in the Supplementary Material available online at <https://doi.org/10.1017/S0016756820001211>); Tang *et al.* 2013), indicating contemporaneous emplacement of dolerite dykes and the Ledong granodiorite–diorite.

4. Geochemical and isotopic character of Mesozoic magmatic suites on Hainan and in SE China

The Mesozoic intrusive suites on Hainan are geochemically and isotopically distinct from each other, and the timing of their emplacement represents discrete tectonomagmatic episodes (Table 1). Triassic rock suites (Xinglong dolerite, Xinglong granite, Wanning gabbro and Fenjiezhou syenite) are predominantly alkaline in nature (Fig. 5). SiO_2 contents of the Xinglong dolerite and granite show a bimodal distribution, ranging between 48.3 and 49.0 wt %, and 75.2 and 77.00 wt %, respectively. The Al_2O_3 content of the Xinglong dolerite is significantly higher than that of the Xinglong granite, and the alkali ($\text{Na}_2\text{O} + \text{K}_2\text{O}$) contents for both rock types are high (8.7–8.9 wt %). The Xinglong granite is high-K and has low rare earth elements (REE) concentration. It is strongly enriched in light REE (LREE), but weakly enriched in heavy REE (HREE) on a chondrite-normalized REE diagram (Fig. 9a). It also shows significant Eu anomalies ($\text{Eu}/\text{Eu}^* = 0.38\text{--}0.41$) (Fig. 9a). On a MORB-normalized multi-element diagram, the Xinglong granite

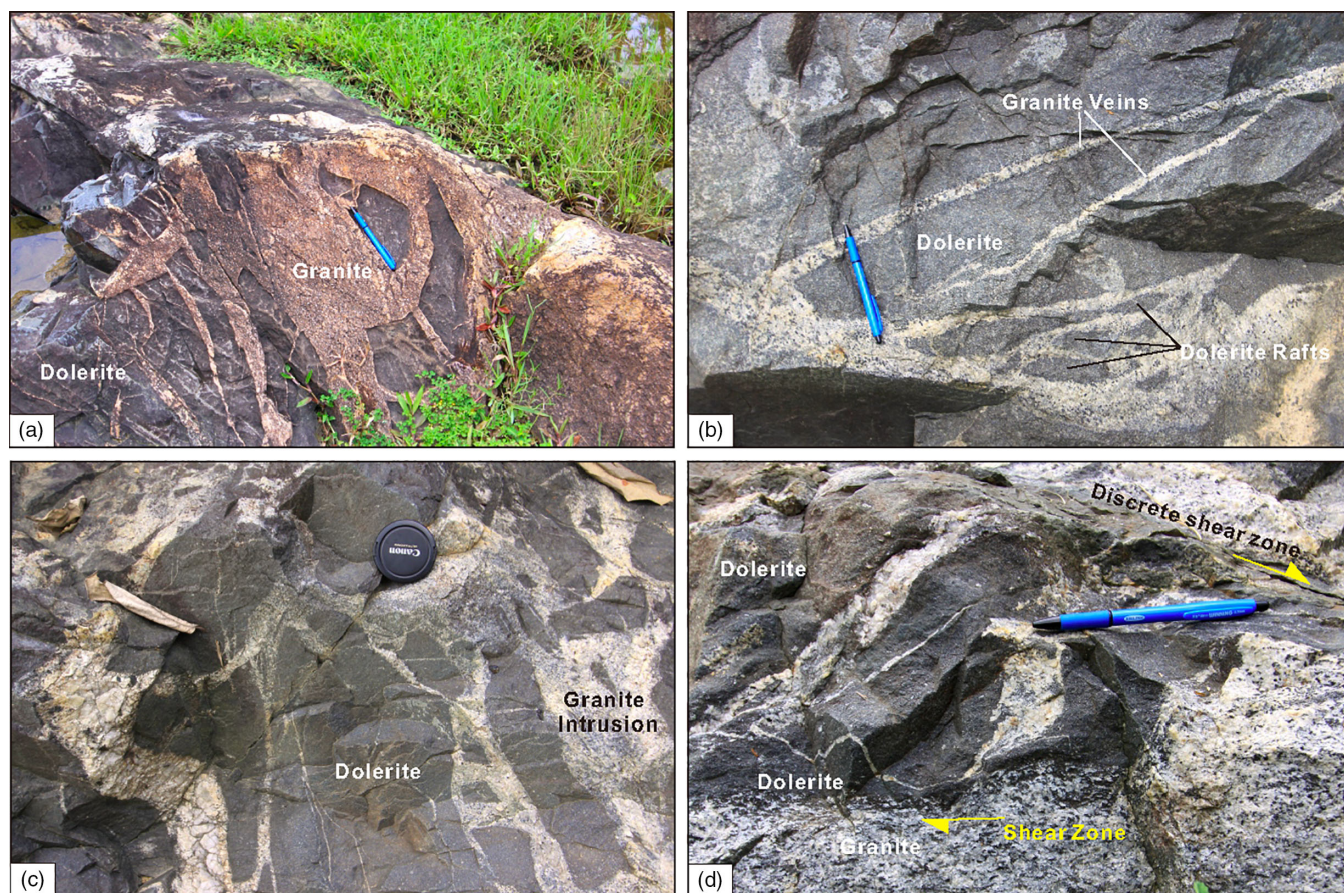


Fig 6. Outcrop images of the primary intrusive relationships between the Triassic Xinglong granite and dolerite. (a–c) Xinglong granite is intrusive into the dolerite, forming jigsaw puzzle rafts of angular mafic rock pieces floating in the felsic rock, typical of magma stoping. (d) Syn-kinematic intrusion of the Xinglong granite along extensional shear zones in the dolerite.

samples are characterized by enrichment in Y and Yb, and depletion in Sr, Ba, P and Ti (Fig. 9b). The Xinglong granite represents an I-type granite (Fig. 9). The slightly older, hypabyssal Xinlong doleritic rocks contain abundant amphibole, and are enriched in both LREE and large-ion lithophile elements (LILE; Rb, Ba, Th, K) (Fig. 9b). They are depleted in high-field strength elements (HFSE; Nb, Ta, Ti; Fig. 9b). The close association of these dolerite rock samples with the garnet–lherzolite melting curve on the Sm/Yb vs La/Yb and Sm/Yb vs La/Sm diagrams (Fig. 10) suggests that their magmas were derived from partial melting of lherzolitic peridotite of a continental mantle lithosphere in or near the garnet stability field. The slightly younger Fenjiezhou syenite (231 ± 3.4 Ma) is an A-type pluton, also showing LREE and LILE enrichments (Fig. 9a, b).

Cretaceous dykes and the coeval Ledong granodiorite are subalkaline in nature (Fig. 5), amphibole-rich (Fig. 7d) and show significant enrichment in LREE and LILE (Sr, K, Rb, Ba, Th) and depletion in HFSE in both chondrite-normalized and MORB-normalized multi-element diagrams (Fig. 9). We have plotted the Cretaceous Jinjiang and Yuebei dykes and the Cretaceous Matou monzogranite from mainland China on the chondrite-normalized and MORB-normalized multi-element diagram for comparison (Fig. 9a); these Cretaceous intrusive suites from SE China and our samples of the Cretaceous dyke swarms on Hainan display similar LREE and LILE enrichment patterns. These geochemical features are characteristic of magmas derived from partial melting of subduction-modified peridotites (Ulmer, 2001).

Initial $^{87}\text{Sr}/^{86}\text{Sr}$ vs $^{143}\text{Nd}/^{144}\text{Nd}$ isotopic values of the representative rock suites (Fig. 11) show a well-defined pattern of a time-progressive evolution of melt sources from a highly enriched EMII-type mantle (for the Triassic magmatic series) toward a sub-arc type mantle field (for the Cretaceous dyke intrusions). Triassic granite–dolerite and gabbro–syenite rocks plot close to the EMII field, whereas the Jurassic gabbros and Cretaceous granitic plutons and dolerite–microgabbro dyke swarms plot within the sub-arc mantle field (Fig. 11). This trend reflects the geochemical evolution of the subduction-conditioned, subcontinental lithospheric mantle (SCLM) beneath SE China throughout the Mesozoic (Zhou *et al.* 2015). Similar SCLM metasomatism and geochemical evolution patterns have also been documented from Mesozoic E-NE China (Liu *et al.* 2006; Zheng *et al.* 2018, and references therein; Wang *et al.* 2019).

5. Structural architecture and magmatic make-up of Mesozoic SE China

Figure 12 summarizes the Mesozoic regional geology, geochemical affinity and tectonic settings of magmatism on Hainan and in SE China. Also depicted in this diagram are the tectonostratigraphy and structural architecture of the Mesozoic sedimentary and volcanic rock sequences. The regional geology patterns and tectonostratigraphic units show a major change from contraction to extension in the Middle Mesozoic, attended by magmatism with different geochemical signatures.

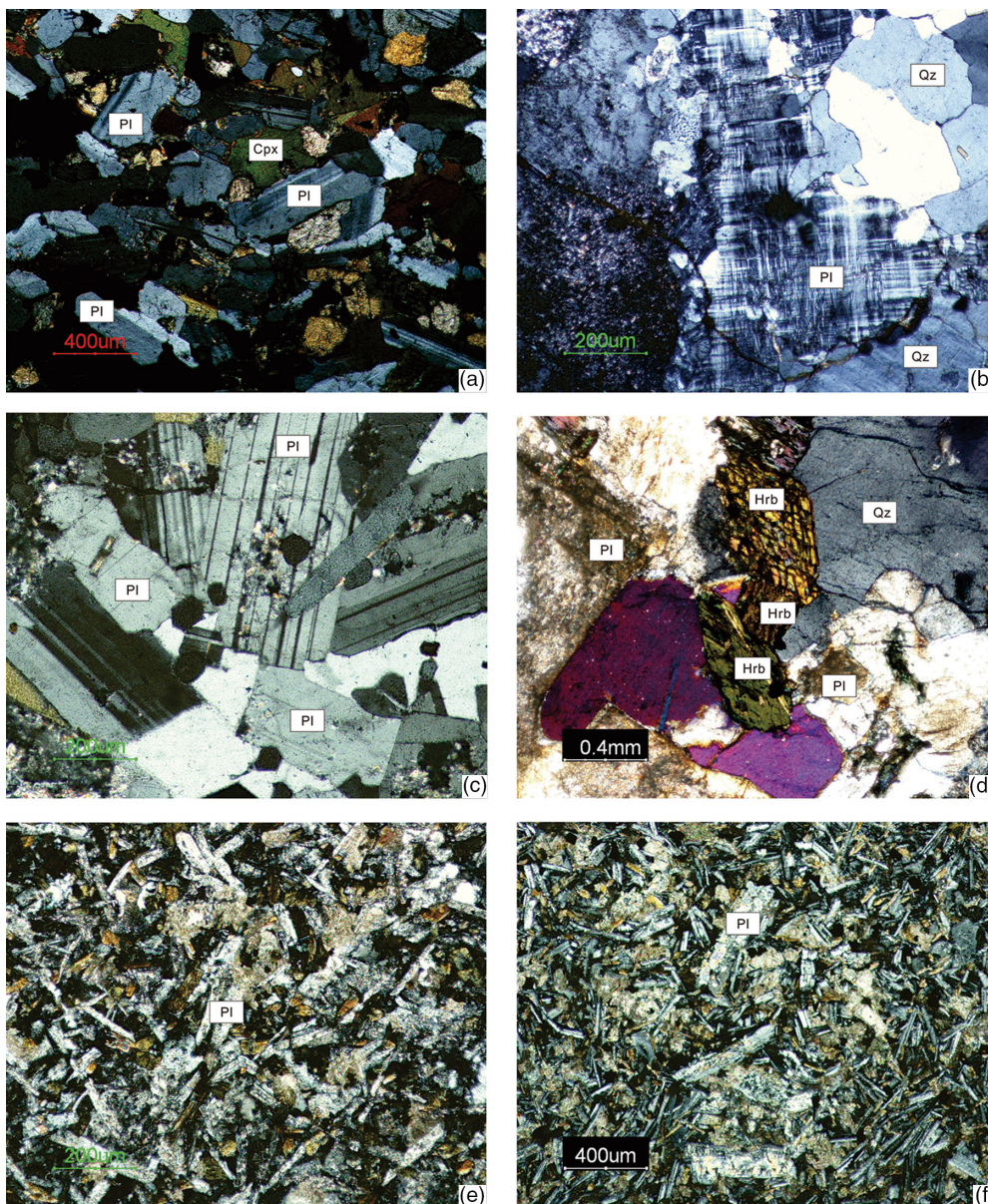


Fig 7. Microphotographs of representative samples from: (a) Xinglong dolerite; (b) Xinglong granite; (c) Wanning gabbro (coarse-grained) with euhedral to subhedral and prismatic plagioclase crystals with Carlsbad-albite twins; (d) Ledong diorite; (e) Wenshi dykes; (f) Sanya dykes. Key for acronyms: Cpx – clinopyroxene; Hrb – hornblende; Qz – quartz; Pl – plagioclase. See the text for descriptions of the mineralogy and textures of these rock samples.

5.a. Triassic geology and magmatism

Lower Triassic shallow marine rocks rest unconformably on the Permo-Carboniferous sedimentary and volcanic units. In the Zhejiang region, for example, the Lower Triassic Changxing Formation includes black bioclastic limestones with graded-bedding and cross-bedding features, characteristic of high-energy, shallow marine deposits, and the Lower Triassic Zhengtang Formation further south consists of clastic and carbonaceous turbiditic sequences; collectively, these two formations represent shelf-break and continental slope deposits, and are deformed by NW-vergent folds and thrust faults (Xiao & He, 2005; Chu *et al.* 2012). These deformed Lower Triassic rocks are unconformably overlain by Upper Triassic lacustrine and terrestrial rocks that are interpreted as foreland basin (Li & Li, 2007) or molasse deposits (Xiao & He, 2005).

Triassic sedimentary strata and some of the NW-vergent thrust faults are cross-cut by high-K, I-type granitoid, gabbro, syenite and

hypabyssal dolerite intrusions (Fig. 12a). The negative $\varepsilon_{Nd}(T)$ values (-5.90 to -3.86) of the granite and dolerite rocks suggest partial melting of an enriched mantle source (EMII), accompanied by high- T crustal melting for the origin of their magmas (Fig. 11). Granitoid plutons and thrust faults become younger to the NW (249 to 217 Ma; Fig. 3), in the direction of thrusting, as documented by U–Pb zircon SHRIMP and $^{40}\text{Ar}/^{39}\text{Ar}$ mica ages of representative rocks (for a comprehensive age data table, see the data repository Files in Li & Li, 2007). This early Mesozoic regional structure is known as the SE China Fold and Thrust Belt (Fig. 3; Xiao & He, 2005).

5.b. Jurassic geology and magmatism

Jurassic volcanic and sedimentary rock sequences in SE China rest unconformably on the folded–faulted Triassic foreland basin strata and deformed granitoids (Fig. 12b) or on the deformed Devonian to Carboniferous siliciclastic rock assemblages. The Jurassic magmatism produced A- and I-type granitoids, alkaline granites and

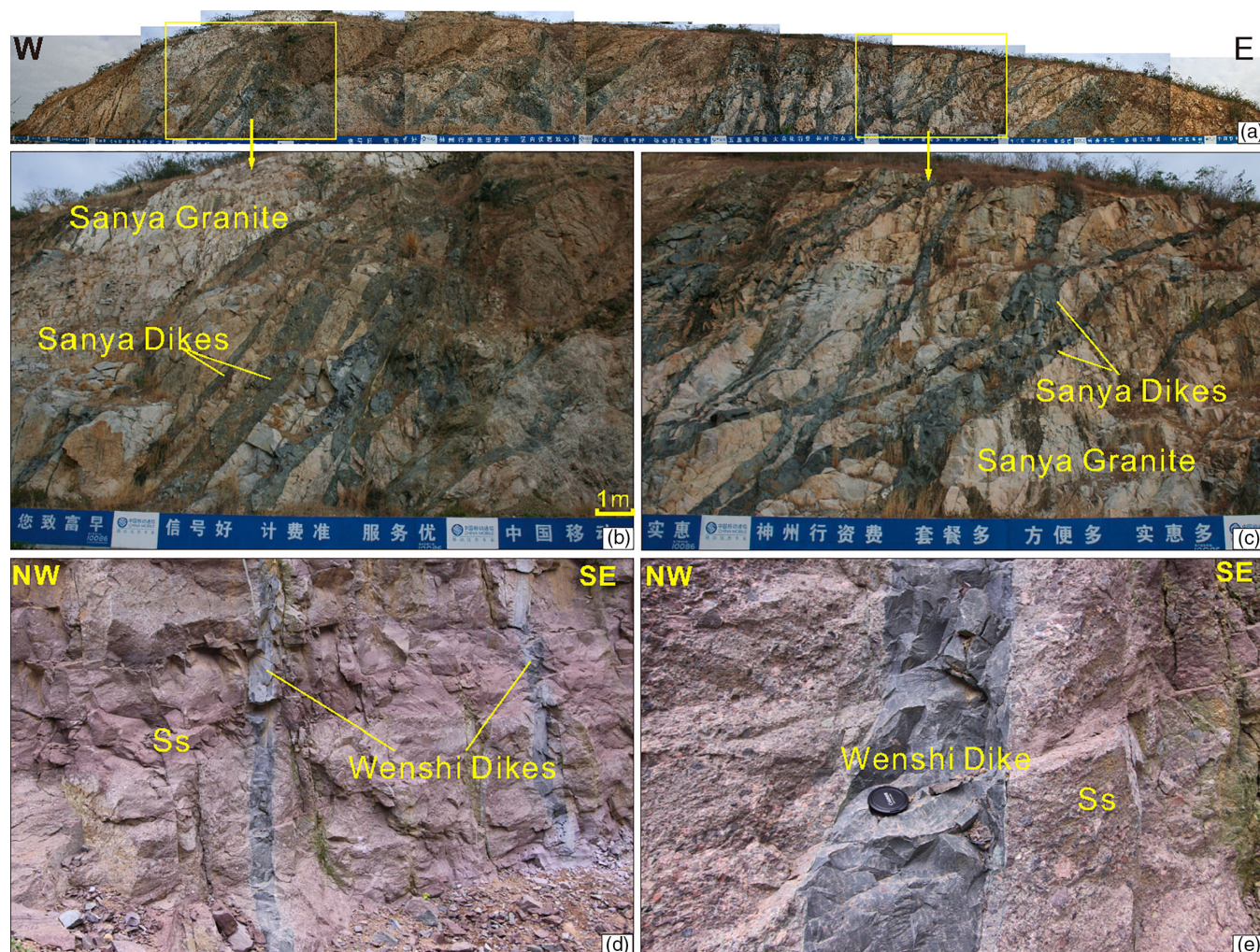


Fig 8. Outcrop images of the Cretaceous Sanya dykes with their granitic host rock (Sanya granite) and the Cretaceous Wenshi dykes with their Cretaceous red sandstone host. Sanya dykes were emplaced along NE–SW-striking extensional fractures and fault systems that show consistently top-to-the west displacement and shearing.

syenites with minor gabbro, diorite, dolerite and lamprophyre dyke intrusions, which were emplaced along NE–SW-trending extensional fault systems (YH Jiang *et al.* 2006; XM Zhou *et al.* 2006; C Guo *et al.* 2012; Quelhas *et al.* 2020). These plutons locally intruded into thick sequences of basaltic, dacitic, rhyolitic volcanic rocks and alkaline basalts, which were also erupted within NE–SW-oriented grabens (Fig. 12b; Li *et al.* 2010; C Guo *et al.* 2012; Wei *et al.* 2018). The Jurassic magmatism was hence associated with extensional deformation in a ~400 km wide belt, characterized by a Basin and Range-type crustal structure, which included lacustrine–playa lake deposits, evaporites and alluvial fan systems interspersed with bimodal volcanic sequences (see Wang & Shu (2012), and references therein, for an overview of the distribution of Mesozoic metamorphic core complexes in SE China, and Ni *et al.* (2013) for the occurrence of a metamorphic core complex in E China).

Jurassic granites have a relatively wide range of $\epsilon_{\text{Nd}}(T)$ values (–6.55 to –0.78) and are geochemically similar to A-type granites (Fig. 11). However, geochemical compositions and isotopic fingerprints of these A-type granites display major differences, which appear to have resulted from isotopically distinct crustal domains within the South China Block, particularly in Cathaysia (Quelhas *et al.* 2020). Syenites have high K contents (shoshonitic) and a large range of Nd–Sr isotopic compositions ($\epsilon_{\text{Nd}}(T) = -3.54$ to $+3.44$).

Gabbros are geochemically analogous to intraplate transitional basaltic rocks and display a narrow range of $\epsilon_{\text{Nd}}(T)$ values (–0.8 to $+0.55$). These geochemical and isotopic features suggest that magmas of the gabbros and syenites were derived from partial melting of a continental lithospheric mantle, which was modified by OIB-type (aesthenospheric) melts (Jiang *et al.* 2006), whereas the granites were produced by magmas that formed from partial melting of hornblende-bearing crustal rocks (Li *et al.* 2010; Yao *et al.* 2017; Quelhas *et al.* 2020).

5.c. Cretaceous geology and magmatism

Cretaceous plutonic and volcanic rocks occur in a NE–SW-trending belt (Figs 2, 3). Granites and rhyolites within a 300 km wide zone adjacent to the modern coastline form coeval, felsic intrusive and extrusive assemblages with a minor occurrence of gabbros and basalts. Dominantly composed of high-K, I-type and A-type granites, the Cretaceous granitoids in SE China were emplaced in multiple episodes within discrete time windows (Li, 2000; XY Li *et al.* 2019; X Zhao *et al.* 2019). The 146–136 Ma and 132–123 Ma granites were intruded in southern Anhui, Jiangsu, Zhejiang and northern Jiangxi provinces (Gao *et al.* 2019b), whereas the 109–101 Ma high-K, calc-alkaline I-type granites were emplaced near the modern

Table 1. Sr and Nd isotope ratios of the representative Triassic, Jurassic and Cretaceous intrusive suites in Hainan – SE China

| Sample No. | Rock type | Age | $^{87}\text{Sr}/^{86}\text{Sr}(2\sigma)$ | $^{143}\text{Nd}/^{144}\text{Nd}(2\sigma)$ | Location | Reference |
|------------|-----------|--------|--|--|-------------------|-------------------------|
| WS02 | Dolerite | 110 Ma | 0.706407 ± 9 | 0.512612 ± 8 | Wenshi, Hainan | This study |
| WS03 | Dolerite | 110 Ma | 0.706358 ± 11 | 0.512607 ± 10 | Wenshi, Hainan | This study |
| CH04 | Dolerite | 94 Ma | 0.705526 ± 8 | 0.512637 ± 10 | Chahe, Hainan | This study |
| CH07 | Dolerite | 94 Ma | 0.705345 ± 12 | 0.512629 ± 8 | Chahe, Hainan | This study |
| SY1 | Dolerite | 93 Ma | 0.708441 ± 20 | 0.512446 ± 9 | Sanya, Hainan | Ge 2003 |
| SY2 | Dolerite | 93 Ma | 0.708597 ± 17 | 0.512420 ± 8 | Sanya, Hainan | Ge 2003 |
| SY3 | Dolerite | 93 Ma | 0.708341 ± 13 | 0.512433 ± 11 | Sanya, Hainan | Ge 2003 |
| SY4 | Dolerite | 93 Ma | 0.708157 ± 24 | 0.512445 ± 9 | Sanya, Hainan | Ge, 2003 |
| SY5 | Dolerite | 93 Ma | 0.709141 ± 17 | 0.512442 ± 8 | Sanya, Hainan | Ge, 2003 |
| SY6 | Dolerite | 93 Ma | 0.708630 ± 20 | 0.512435 ± 13 | Sanya, Hainan | Ge, 2003 |
| SY7 | Dolerite | 93 Ma | 0.708363 ± 23 | 0.512471 ± 3 | Sanya, Hainan | Ge, 2003 |
| QZ-1 | Gabbro | 109 Ma | 0.705590 ± 13 | 0.512488 ± 13 | Quanzhou, Fujian | Z Li <i>et al.</i> 2012 |
| QZ-2 | Gabbro | 109 Ma | 0.705732 ± 15 | 0.512434 ± 8 | Quanzhou, Fujian | Z Li <i>et al.</i> 2012 |
| QZ-3 | Gabbro | 109 Ma | 0.705653 ± 14 | 0.512479 ± 10 | Quanzhou, Fujian | Z Li <i>et al.</i> 2012 |
| QZ-6 | Gabbro | 109 Ma | 0.705691 ± 13 | 0.512451 ± 9 | Quanzhou, Fujian | Z Li <i>et al.</i> 2012 |
| Qf-1 | Gabbro | 108 Ma | 0.707904 ± 11 | 0.512445 ± 10 | Quanzhou, Fujian | Zhou & Chen, 2001 |
| HC-2 | Gabbro | 111 Ma | 0.705581 ± 12 | 0.512468 ± 8 | Huacuo, Fujian | Z Li <i>et al.</i> 2012 |
| HC-3 | Gabbro | 111 Ma | 0.705831 ± 15 | 0.512423 ± 9 | Huacuo, Fujian | Z Li <i>et al.</i> 2012 |
| 2KGN29-1 | Gabbro | 173 Ma | 0.708413 ± 10 | 0.512613 ± 18 | Chebu, Jiangxi | Li <i>et al.</i> 2010 |
| 2KGN29-4 | Gabbro | 173 Ma | 0.708105 ± 13 | 0.512567 ± 17 | Chebu, Jiangxi | Li <i>et al.</i> 2010 |
| 2KGN29-5 | Gabbro | 173 Ma | 0.707955 ± 12 | 0.512537 ± 14 | Chebu, Jiangxi | Li <i>et al.</i> 2010 |
| XL15-1 | Dolerite | 238 Ma | 0.712289 ± 9 | 0.512336 ± 5 | Xinglong, Hainan | This study |
| XL16-1 | Granite | 234 Ma | 0.715653 ± 9 | 0.512197 ± 8 | Xinglong, Hainan | This study |
| WN03 | Gabbro | 240 Ma | 0.706706 ± 9 | 0.512593 ± 8 | Wanning, Hainan | This study |
| 97HN114 | Granite | 237 Ma | 0.716775 ± 13 | 0.512244 ± 14 | Qiongzong, Hainan | Ge, 2003 |
| 99HN211 | Granite | 237 Ma | 0.713691 ± 16 | 0.512071 ± 13 | Qiongzong, Hainan | Ge, 2003 |
| 99HN30 | Granite | 237 Ma | 0.713976 ± 16 | 0.512087 ± 12 | Qiongzong, Hainan | Ge, 2003 |
| 99HN411 | Granite | 237 Ma | 0.713354 ± 20 | 0.512039 ± 13 | Qiongzong, Hainan | Ge, 2003 |
| 99HN363 | Granite | 237 Ma | 0.716599 ± 16 | 0.512046 ± 14 | Qiongzong, Hainan | Ge, 2003 |
| 99HN452 | Granite | 237 Ma | 0.715264 ± 20 | 0.512081 ± 13 | Qiongzong, Hainan | Ge, 2003 |
| 99HN52 | Granite | 237 Ma | 0.712107 ± 14 | 0.512103 ± 14 | Qiongzong, Hainan | Ge, 2003 |

coastline of SE China (Z Li *et al.* 2012). The younger, 97–87 Ma calc-alkaline I-type granites and some A-type granites were emplaced in coastal Fujian and eastern Taiwan (Li, 2000; X Zhao *et al.* 2019). Cretaceous granites in Fujian, Guangdong and Zhejiang provinces that are closer to the present coastline are spatially associated with monzogranite, biotite granite, hornblende gabbro and syenite, and have I-type geochemical characteristics with enrichment in LREE and LILE, and relative depletion in HFSE (Fig. 9; Lapiere *et al.* 1997; Guo *et al.* 2012a, b; Z Li *et al.* 2012; Tao *et al.* 2020). These rocks have a relatively narrow and homogeneous Sr–Nd isotopic compositional range, showing small negative $\epsilon_{\text{Nd}}(T)$ values (–4.1 to –2.2) (Fig. 12c).

Cretaceous granitoids (132–123 Ma and 117 Ma) further inland in Hunan Province are high-K, calc-alkaline and weakly to strongly peraluminous in character, represented by two-mica or biotite

monzogranites and minor granitoids. They display LREE enrichments and negative Ba, Sr, N, P and Ti anomalies, indicating strong subduction influence in their melt evolution (Ji *et al.* 2017). Their negative zircon $\epsilon_{\text{Hf}}(t)$ values (–12.5 to –3.6) and crustal Hf model (T_{DM}) ages (1.4–2.0 Ga), combined with other geochemical features are interpreted to indicate partial melting of Neoproterozoic metapelitic rocks of the South China Block as their magma source (Ji *et al.* 2017). Further to the E-NE in Jiangxi and Anhui provinces the Early Cretaceous granitoid plutons (i.e. Lingshan pluton in the Gan-Hang belt and Huayuan-gong granitoids in the Lower Yangtze River Belt) display A-type geochemical affinities with metaluminous to weakly peraluminous compositions, enriched Hf isotope ratios of zircon and a large range of high Y/Nb ratios (Yang *et al.* 2017; Wang *et al.* 2018). Magmas of these A-type plutons were derived from mixing of aethenospheric melts

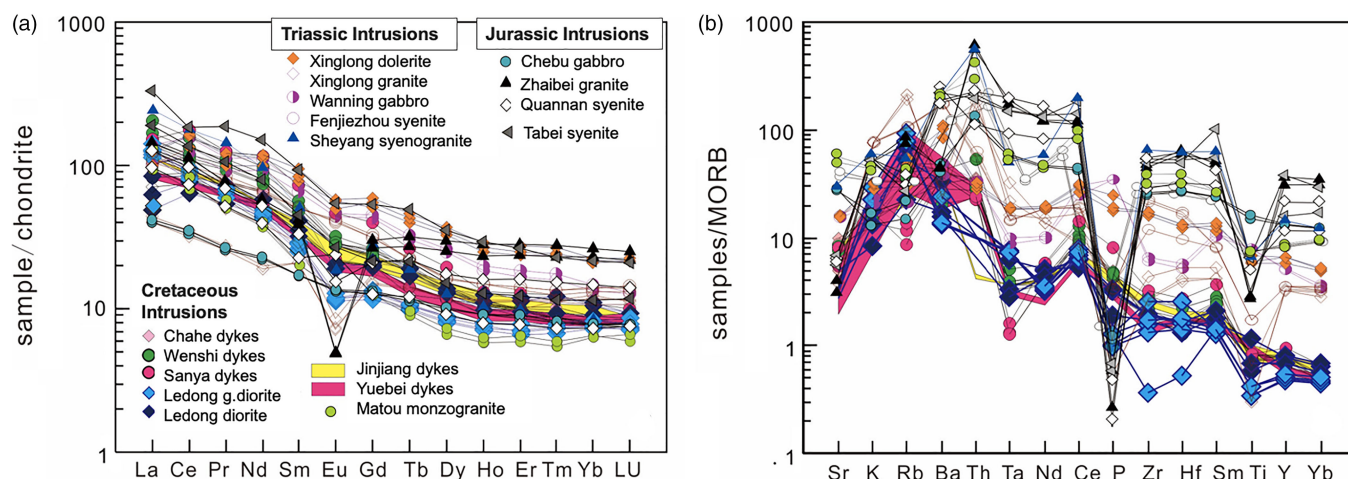


Fig 9. (a) Chondrite-normalized REE diagram of representative Triassic, Jurassic and Cretaceous intrusions on Hainan and in SE China; (b) MORB-normalized multi-element diagram of representative Triassic, Jurassic and Cretaceous intrusions on Hainan and SE China. FJZ = Fenjiezhou syenite. Chondrite values are taken from Boynton (1984). MORB values are taken from Pearce (1982, 1983). Data for the following intrusions are from Triassic Sheyang syenogranite (Zhu *et al.* 2017); Jurassic Chebu gabbro (He *et al.* 2010; XH Li *et al.* 2010), Zhaibei granite (XH Li *et al.* 2010), Quannan syenite (XH Li *et al.* 2010) and Tabei syenite (XH Li *et al.* 2010); Cretaceous Jinjiang dykes (Z Li *et al.* 2012), Yuebei dykes (Qi *et al.* 2012) and Matou monzogranite (Liu *et al.* 2014).

with magmas originated from partial melting of sedimentary rocks of a Mesoproterozoic crystalline basement (Yang *et al.* 2017; Wang *et al.* 2018).

Cretaceous volcanic rocks near the coastal regions in SE China fall into two broad time intervals. The 143–124 Ma, acidic- to intermediate-composition volcanic rocks show variable enrichment in K, Rb, Ba, Th and Ce, and negative Nb, Ta, Zr, Hf and Yb anomalies. Geochemically, these volcanic rocks are similar to the age-equivalent, first and second episode, I-type granitic plutons in the region. This phase of volcanism in SE China also coincided with extensive ignimbrite flare-up episodes and with the formations of nested caldera complexes above large, overlapping silicic magma chambers near the modern shorelines in SE China (for example, in Fujian (Qiu *et al.* 1999); in Western Guangdong (Geng *et al.* 2006); in Jiangxi (Yang *et al.* 2011); and in Hong Kong (Sewell *et al.* 2012)). Thus, it appears that the Early Yanshanian magmatic phase in SE China culminated in a ‘surge of pulsed supereruptions’ during the latest Jurassic – Early Cretaceous (Sewell *et al.* 2012, p. 15), reminiscent in scale of the Yellowstone Caldera collapses in the Western USA during the Quaternary (Vazquez & Reid, 2002). The 97–88 Ma bimodal volcanic rock suites exhibit significant negative Nb anomalies and negative $\epsilon_{\text{Nd}}(T)$ values, suggesting that their magmas were derived from partial melting of an enriched lithospheric mantle source (Li, 2000; XY Li *et al.* 2018).

Cretaceous volcanic rocks occurring further inland from the coastal regions are composed of tholeiitic and OIB-type basalts and minor alkaline rhyolites (YM Wu *et al.* 2020), interlayered with red sandstone, siltstone and mudstone, all deposited in NE–SW-oriented normal fault-bounded basins (Lapierre *et al.* 1997; Y Wang *et al.* 2020). The geochemical and isotopic nature of these tholeiitic basalts suggests that their magmas were derived from a combination of asthenospheric decompression melting and low-pressure, lower crustal melting in a continental setting (Fig. 12c). The 90 Ma Ji’an basalts in central Jiangxi Province have OIB-like geochemical signatures and display Sr–Nd–Pb–Hf isotopic compositions characteristic of a depleted asthenospheric mantle, which was enriched by melts derived from dehydration of a subducted oceanic crust (Wu *et al.* 2020).

Syn-volcanic Cretaceous sedimentary rocks represent fluvial to lacustrine deposits, formed in a broad intracontinental rift system. This regional extensional structure represents the *East China Rift System* (Fig. 3; Tian *et al.* 1992). Cretaceous plutonic rocks and their volcanic counterparts within the East China Rift System represent the products of magmas, which were derived from partial melting of a subduction-metasomatized SCLM and which were variously affected by crustal contamination. NE–SW-running 101–93 Ma doleritic dyke swarms on Hainan reflect a discrete pulse of hypabyssal mafic magmatism during the Late Cretaceous, consistent with the geometry and kinematic evolution of the East China Rift System. Cretaceous mafic dyke intrusions with a predominant NE–SW orientation and age clusters of ~140 Ma, ~105 Ma and ~90 Ma also occur in Guangdong and Fujian, and display tholeiitic geochemical affinities (Li & McCulloch, 1998). These extensive NE–SW-striking doleritic dyke swarms near the coastal areas and the NE–SW-running East China Rift System point to a NW–SE-oriented tensile stress regime and the associated extensional deformation phase in SE China during the Cretaceous.

In summary, rifting, crustal subsidence, extensional doming and exhumation were widespread in the South China Block, particularly within Cathaysia during the Cretaceous (Figs 2, 3). The timing of the NW–SE-directed extension in Cathaysia has been constrained as 136–80 Ma based on thermochronological studies (Li, 2000; Zhou & Li, 2000; Li *et al.* 2014). The results of these studies also indicate that the Cretaceous extensional tectonics and its attendant magmatism in Cathaysia migrated to the SE (oceanward in the present coordinate system) through time (Li, 2000; Li *et al.* 2014, 2016; Yang *et al.* 2017; Wang *et al.* 2018, 2020).

6. Crustal and mantle structure beneath modern SE China

The crustal make-up and architecture of SE China display major differences from north to south across the Jiang Shao Fault between the Yangtze and Cathaysia blocks (Figs 2, 3) and also from west to east within Cathaysia, as determined by combined gravity, P- and S-wave velocity, magnetotelluric, mass density and heat flow measurements (Ai *et al.* 2007; Lin *et al.* 2018; YF Zhang

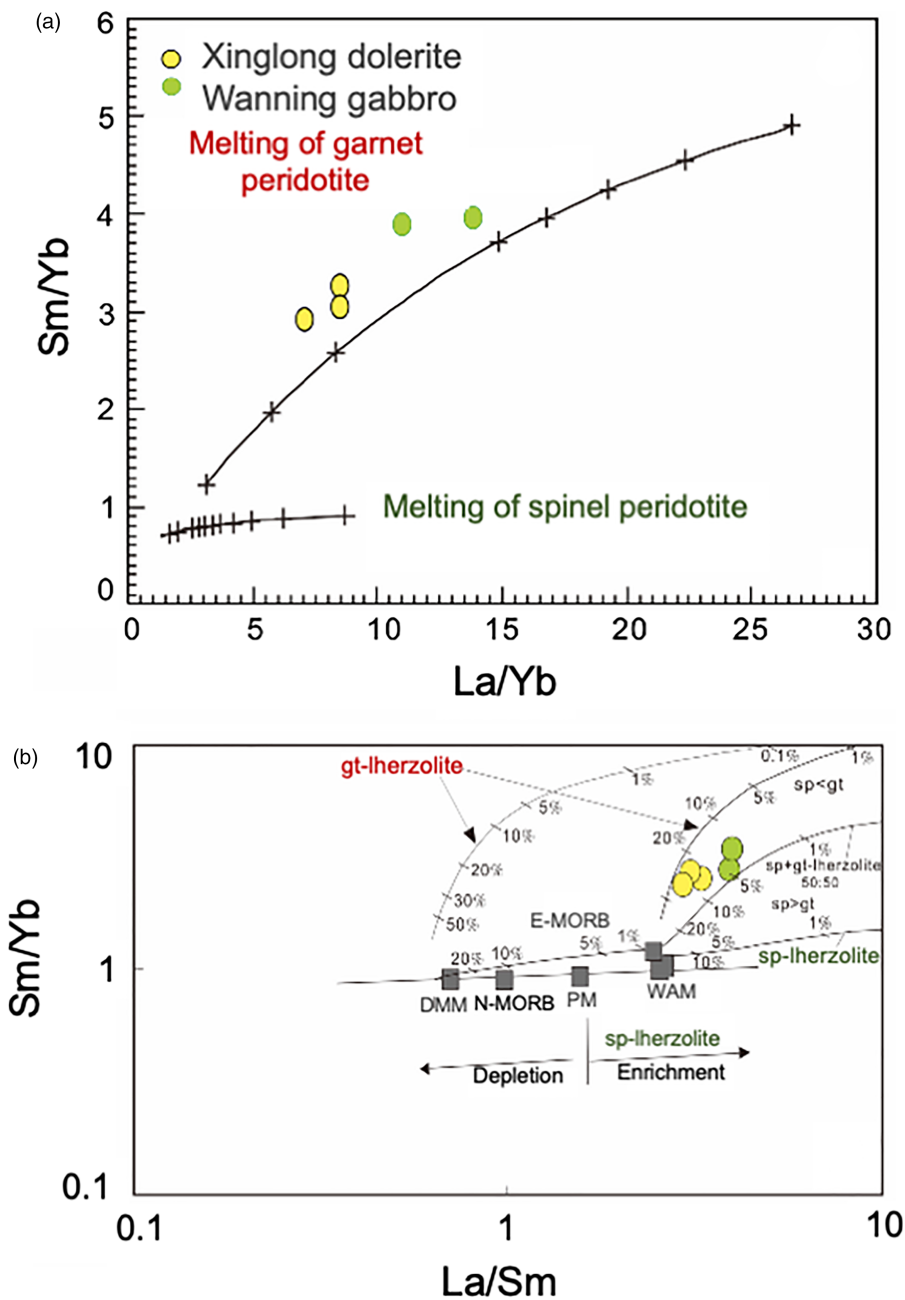


Fig 10. (a) Plot of the Sm/Yb vs La/Yb compositional variations of the Xinlong dolerite and Wanning gabbro. Melting curves are from Xu *et al.* (2005); (b) plot of the Sm/Yb vs La/Sm compositional variations of the Xinlong dolerite and Wanning gabbro. Melting curves are from Aldanmaz *et al.* (2000). DMM = depleted MORB mantle, E-MORB = enriched mantle, N-MORB = normal MORB, PM = primitive mantle, WAM = Western Anatolian mantle, gt = garnet, sp = spinel. Ticks on the melting curves indicate the same percentages of melt fractions.

et al., 2016; Zhang *et al.* 2020). The results of recent geophysical studies have shown that both the Yangtze and Cathaysia blocks consist of multiple accreted continental and oceanic terranes with significantly different lithologies and ages (Lin *et al.* 2018; Zhang *et al.* 2020). The Yangtze Block has an Archaean–Palaeoproterozoic crystalline basement and a Neoproterozoic fold-and-thrust belt in the SE (Jiangnan belt) that is widely interpreted to mark a collisional event (Li *et al.* 2016). The Jiang Shao fault zone (Fig. 3) represents the tectonic boundary between the Yangtze and Cathaysia blocks. Cathaysia consists of West and East Cathaysia blocks, separated by a Mesozoic strike-slip shear zone (Lin *et al.* 2018). The West Cathaysia Block has no cratonic basement and consists mainly of Neoproterozoic arc–back-arc ophiolites (according to the ophiolite classification scheme of Dilek & Furnes, 2009, 2011, 2014) and metamorphic rocks, whereas the East Cathaysia Block has a cratonic basement and

consists of Palaeoproterozoic metapelites, metaplutonic rocks, felsic metavolcanic rocks and migmatites (Lin *et al.* 2018; K Zhang *et al.* 2020). East Cathaysia also displays, in its SE part by the coast, widespread conductive anomaly and large depth-integrated conductance (K Zhang *et al.* 2020), which points to high heat flow coinciding spatially with the distribution of Cretaceous mafic rocks.

The upper and middle crust in the Yangtze and Cathaysia blocks are made of granite–granodiorite, biotite gneiss and granite gneiss (Zhao *et al.* 2013). The lower crust in the Yangtze Block consists of biotite gneiss, monzonite gneiss, migmatite, paragneulite and amphibolite, whereas in the Cathaysia Block it is composed mainly of diorite, amphibolite, metabasalt, as well as metarhyolite, mica quartz schist and paragneulite (He *et al.* 2013; Zhao *et al.* 2013; Stern *et al.* 2018; Gao *et al.* 2019a). The Cathaysian crust shows abrupt lateral and vertical variations

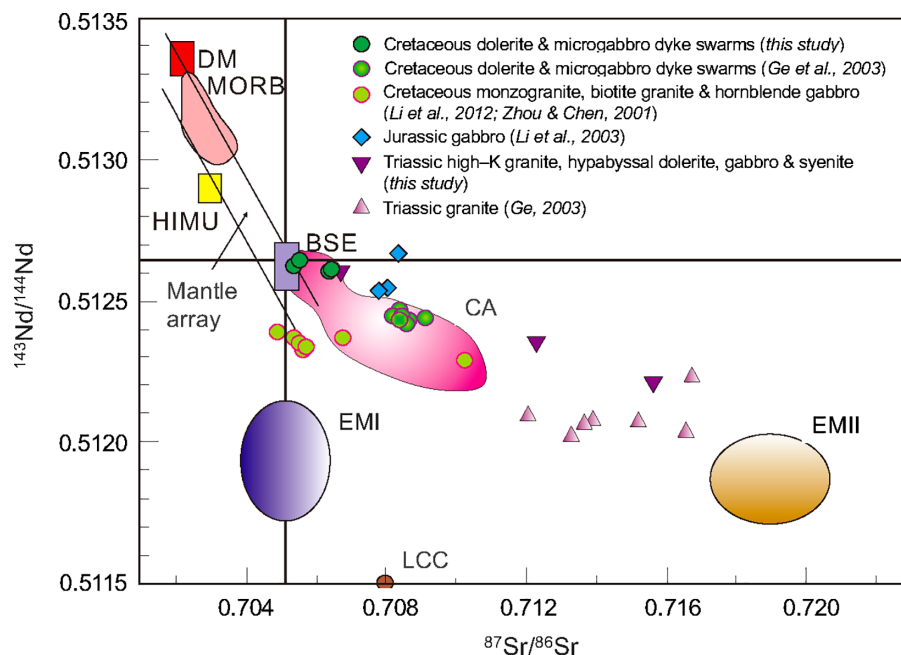


Fig 11. Initial $^{87}\text{Sr}/^{86}\text{Sr}$ vs $^{143}\text{Nd}/^{144}\text{Nd}$ isotope diagram for the representative Mesozoic intrusive suites on Hainan and in SE China. BSE – bulk silicate earth; CA – calc-alkaline field; DM – depleted mantle; EMI – enriched mantle I; EMII – enriched mantle II; HIMU – high ($^{238}\text{U}/^{204}\text{Pb}$) mantle; LCC – lower continental crust; MORB – mid-ocean ridge basalt. Approximate fields of mantle reservoirs and MORB are from Zindler & Hart (1986); the LCC are from Escrig *et al.* (2004).

in lithological units and structures, as observed on seismic profiles and magnetotelluric profiles, that most likely resulted from significant deformation and magmatic reworking, in addition to its accretionary history involving different lithospheric blocks (B Zhao *et al.* 2013; L Zhao *et al.* 2015). The average crustal thickness in Fujian Province in SE Cathaysia is ~ 31 km, and the Moho depth shallows gradually towards the northern South China Sea border (Zhang & Wang, 2007). The entire lithospheric thickness beneath SE China thins towards the South China Sea (Dong *et al.* 2018), with the lithosphere–aesthenosphere boundary located at a depth of 60 to 70 km (Q Li *et al.* 2013). Studies of mantle xenoliths recovered from the Cenozoic Xinchang basalts (Zhejiang Province) and Mingxi basalts (Fujian Province) in SE Cathaysia have shown that the Precambrian lithospheric mantle beneath this region was removed and replaced by hotter, younger and fertile mantle during the late Mesozoic lithospheric extension (CZ Liu *et al.* 2012, 2017). This new lithospheric mantle was significantly modified by subduction–related metasomatic processes and upwelling asthenosphere in the latest Mesozoic (Y Xiao *et al.* 2019).

Seismic tomography studies in SE China have shown high V_p – V_s anomalies and low V_p/V_s ratios in the mantle transition zone (MTZ) beneath the Yangtze Block, but low velocity anomalies (particularly very low V_s velocities) and high V_p/V_s ratios in the MTZ beneath the Cathaysia Block (Zhang *et al.* 2016). The large V_s anomalies in the Cathaysia MTZ may point to the existence of lower-viscosity partial melting products in the upper mantle of Cathaysia (Fig. 2); the high V_p – V_s anomalies in and across the MTZ of the Yangtze Block are likely to point to the existence of a cold slab (proto-Pacific?) beneath Yangtze (Zhang *et al.* 2016). Seismic tomographic data also reveal that there are no detectable anomalies, signalling the existence of a subducted/accreted oceanic plateau or continental fragment beneath SE China (Li & van der Hilst, 2010; Li *et al.* 2013; Zhang *et al.* 2016).

Based on these crustal and mantle features of the Yangtze and Cathaysia continental blocks, we can make two major deductions: (1) towards the coastal areas in SE China and particularly in SE Cathaysia, depth to the aesthenosphere becomes shallow beneath

the continental lithosphere as a result of significant lithospheric thinning and mantle upwelling in the Late Mesozoic. Furthermore, the continental crust becomes more mafic and magmatically reworked, as observed on magnetotelluric and seismic profiles (Zhao *et al.* 2013; K Zhang *et al.* 2020). Therefore, it appears that the continental lithosphere of SE China was significantly attenuated by the end of the Cretaceous; (2) the continental margin of SE China did not experience accretion of a large oceanic plateau or a microcontinent in the Mesozoic.

7. Geodynamic model

One of the fundamental questions about the Mesozoic tectonics of East Asia is when the subduction of the palaeo-Pacific oceanic plate beneath the Asian continent began. Although previous studies have suggested early Jurassic or later timing of this event, most recent geochemical, geochronological and structural investigations in NE and SE China show that onset of an active margin tectonics and the initiation of subduction of the palaeo-Pacific oceanic lithosphere beneath East China were under way by the early Triassic (Zhou *et al.* 2014; Sun *et al.* 2015; K Liu *et al.* 2017) and perhaps even earlier in the late Permian (Wang *et al.* 2005; Li *et al.* 2006; Zhou *et al.* 2006; Li & Li, 2007; Z-X Li *et al.* 2012; Duan *et al.* 2018; Shen *et al.* 2018). Based on the findings of the work of FQ Zhang *et al.* (2020), our work on Hainan (this study), and the findings of other recent studies (XH Li *et al.* 2012; Egawa, 2013; Domeier & Torsvik, 2014; Shen *et al.* 2018), we postulate a latest Permian–early Triassic start of an active margin tectonics that marked the beginning of the *Pacific Rim of Fire* in its western domain near the eastern margin of East Asia in the western Pacific Ocean (Fig. 13a). Late Permian arc evolution associated with the westward subduction of the palaeo-Pacific oceanic plate has been documented from SE Japan (Hara *et al.* 2018; Zhang X *et al.* 2018) and South Korea (K Yi *et al.* 2012). In our geodynamic model, we envision the South China Block, consisting of the Yangtze and Cathaysia continents, situated in the upper plate of a W-NW-dipping palaeo-Pacific subduction zone (Fig. 13a), and far from the North China and Indochina blocks during the Late Permian (see the palaeogeographic reconstructions of

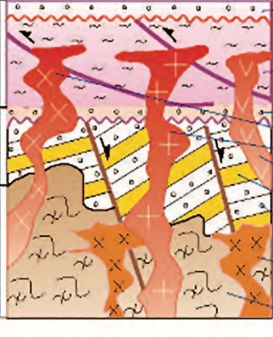
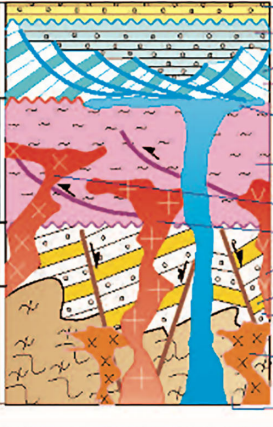
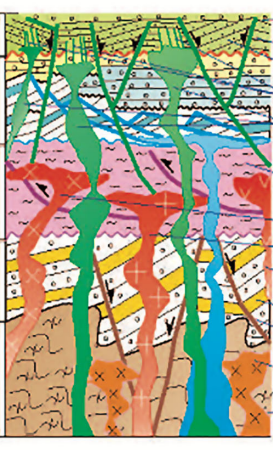
| | Tectonostratigraphy | Regional Geology | Geochemical Affinity of Magmatic Units | Tectonic Setting of Magmatism |
|--|--|---|--|---|
| Proterozoic E. Paleozoic Carbon. Triassic |  <ul style="list-style-type: none"> Shallow-water terrestrial seds. Folded foreland basin seds Salt deposits Gabbro Granitoid Syenite MORB-basalt Rift-deposits Wuzhishan granite (I-type) Crystalline basement | <p>Foreland basin (epieric sea); fold and thrust belt system.</p> | <p>High-K, calc-alkaline, I-type granitoids, gabbros, syenites and mafic hypabyssal rocks (dolerite).</p> <p>$\epsilon_{Nd(T)} = -5.90 \sim -3.86$ (granites and dolerite).</p> | <p>Flat subduction-induced edge flow and asthenospheric uprising.</p> <p>Lithospheric mantle melting, plus high-T/high-P lower crustal melting.</p> |
| Proterozoic E. Paleozoic Carbon. Triassic Jurassic |  <ul style="list-style-type: none"> Lacustrine seds. Clastic rocks Alkaline basalt Bimodal volc. A- and I-type granite, syenites Folded foreland basin seds Gabbro Granitoid Syenite MORB-basalt Rift-deposits Wuzhishan granite (I-type) Crystalline basement | <p>Broad, intra-continental rifting, crustal extension and horst and graben development.</p> <p>Formation of playa lakes and deposition of evaporites and lacustrine sediments.</p> <p>Development of extensive alluvial fan systems.</p> | <p>I- and A-type granites; gabbros and syenites, alkaline basalts and bimodal volcanic rocks.</p> <p>$\epsilon_{Nd(T)} = -6.55 \sim -0.78$ (granites).</p> <p>$\epsilon_{Nd(T)} = -0.82 \sim +0.55$ (gabbros).</p> <p>$\epsilon_{Nd(T)} = -3.54 \sim +3.44$ (syenites).</p> | <p>Asthenospheric upwelling caused by slab foundering-delamination and metasomatism of continental mantle lithosphere by OIB-type melts.</p> <p>Partial melting of this mantle and the Proterozoic-Triassic crustal basement.</p> |
| Proterozoic E. Paleozoic Carbon. Triassic Jurassic Cret. |  <ul style="list-style-type: none"> Fluvial-lacustrine seds. Horst-graben Terrestrial rift deposits Mafic dikes Gabbro-granite, syenite plutons Folded foreland basin seds. Gabbro Granitoid Syenite MORB-basalt Rift-deposits Wuzhishan granite (I-type) Crystalline basement | <p>Lithospheric-scale, regional extension in the SE China Block.</p> <p>Gan-Hang rifting along the Jiang-Shao Fault Zone.</p> <p>Terrestrial depocenters and rifting-related sedimentation above exhumed Precambrian and Triassic basement rocks.</p> | <p>Bimodal gabbro-granite and syenite-granite intrusions.</p> <p>Bimodal volcanic rock suites.</p> <p>Widespread rhyolitic and tuffaceous rocks with minor basaltic lavas (193-130 Ma).</p> <p>$\epsilon_{Nd(T)} = -4.1 \sim -2.2$ (granites).</p> <p>$\epsilon_{Nd(T)} = +0.57 \sim +1.03$ (doleritic dikes).</p> | <p>Steeply-dipping subduction zone beneath the continental margin, and arc-like magmatism near the trench.</p> <p>Asthenospheric decompressional melting beneath the broad backarc region, and low-pressure, lower crustal melting.</p> |

Fig 12. Tectonostratigraphy, regional geology, structural architecture, geochemical affinity – isotopic signatures, and the inferred tectonic settings of Mesozoic tectonomagmatic suites on Hainan and in SE China. Interpreted melt sources and evolution patterns are also shown. Data for the Triassic geology and magmatism are from Li (2002), Xiao & He (2005), Li *et al.* (2006), Li & Li (2007), Hu *et al.* (2017), Yao *et al.* (2017) and this study. Data for the Jurassic geology and magmatism are from Ge (2003), TF Yiu *et al.* (2017), Li *et al.* (2003), Jiang *et al.* (2006), Zhou *et al.* (2006), XH Li *et al.* (2010), Guo *et al.* (2012a, b), Yao *et al.* (2017), Wei *et al.* (2018), Ma *et al.* (2019), and this study. Data for the Cretaceous geology and magmatism are from Lapierre *et al.* (1997), Li (2000), Guo *et al.* (2012a, b), JH Li *et al.* (2014), YZ Yang *et al.* (2017), Wang *et al.* (2018), Gao *et al.* (2019b), Tao *et al.* (2020), D Xu *et al.* (2017), Wang *et al.* (2020) and this study.

Pangaea, Panthalassa, Palaeotethys and Neotethys in Domeier & Torsvik, 2014). The South China and Indochina blocks were separated from the rest of the Pangaea supercontinent by Palaeotethys during this time period.

Although the refined geodynamic model we present here for the Mesozoic evolution of SE China is mechanically similar to that proposed earlier by Li & Li (2007) and ZX Li *et al.* (2012), our

explanation of the kinematics of plate motions, slab dynamics and modes of plate interactions are fundamentally different from their model. Both our model and the model by Li & Li (2007) and ZX Li *et al.* (2012) infer a flat subduction of the palaeo-Pacific oceanic lithosphere in the Permo-Triassic (Fig. 13a). However, the model by Li & Li (2007) proposes an external cause, such as the subduction of a large oceanic plateau on the palaeo-Pacific plate, as the

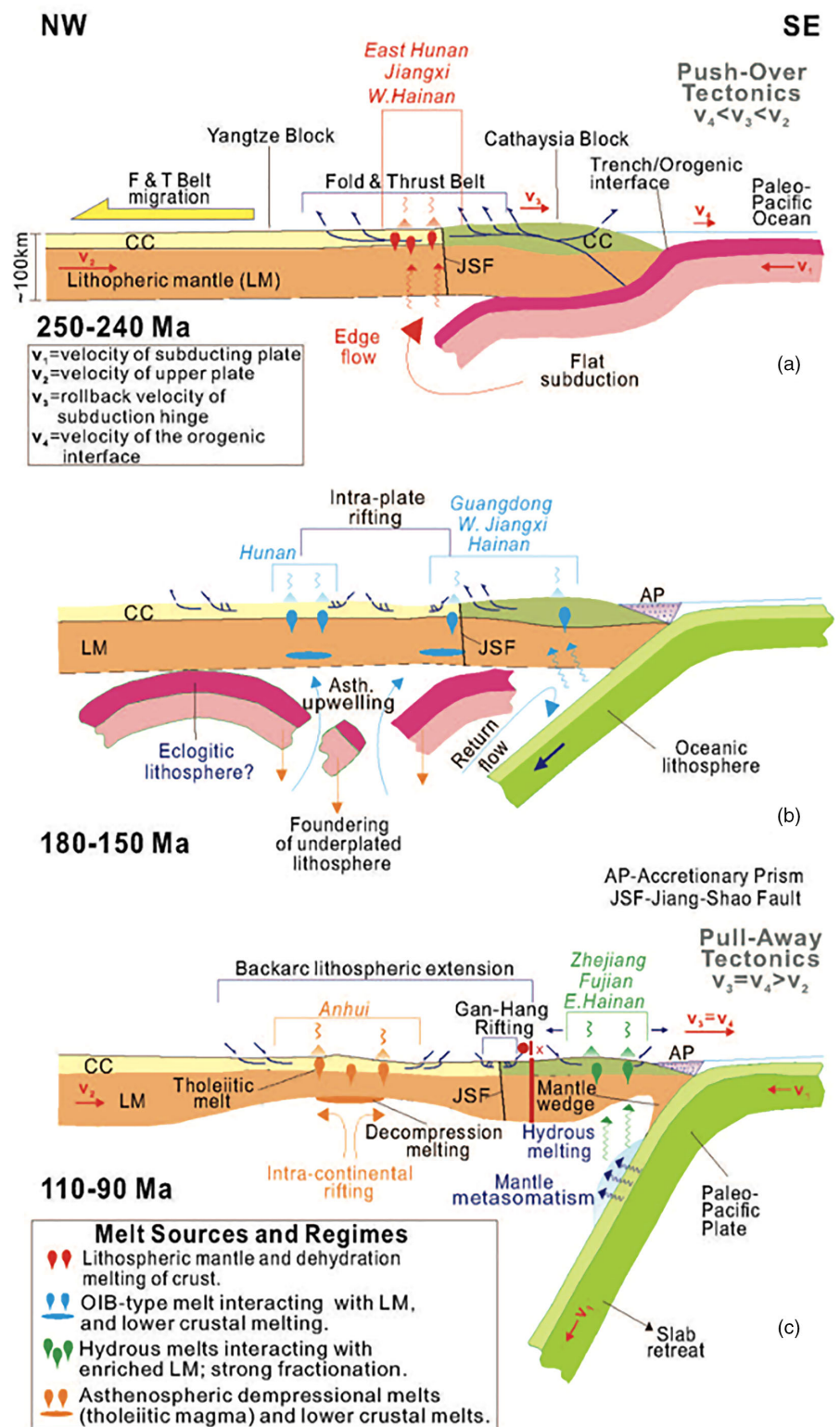


Fig 13. Time-progressive tectonic evolution of Mesozoic SE China through a tectonic mode switch, controlled by slab dynamics of the downgoing palaeo-Pacific Plate and the mantle and upper plate responses to it. AP - accretionary prism; CC - continental crust; JSF - Jian Shao Fault; LM - lithospheric mantle. Data are from Xiao & He (2005), Zhou et al. (2006), Li & Li (2007), ZX Li et al. (2012), Wang et al. (2013), Zhang et al. (2013), J Li et al. (2014), JH Li et al. (2018), N Tao et al. (2019), L Tao et al. (2020), Y Wang et al. (2020) and YM Wu et al. (2020).

driving force for flat slab development. We find no geological or geophysical evidence in the extant literature (i.e. Li & van der Hilst, 2010) for the collision or subduction of a large oceanic plateau along the SE China continental margin during the Permo-Triassic. We suggest that the initial flat subduction was due to a very large width of the subducting palaeo-Pacific slab, as discussed below.

7.a. Onset of active margin tectonics, flat-slab subduction and upper plate deformation

The Late Palaeozoic (Carboniferous to the earliest Permian) tectonics of E-SE China and its continental margin was largely dominated by extensive carbonate platform construction and passive

margin development (FQ Zhang *et al.* 2020, and references therein). This geological process was abruptly halted as the palaeo-Pacific oceanic plate foundered and began to subduct beneath continental Asia towards the end of the Palaeozoic (Fig. 13A). Passive margin transference into an active margin implies spontaneous subduction, but what causes this sudden passive margin collapse is not well understood, and the concept of subduction initiation is the subject of extensive interdisciplinary research (see Stern & Gerya, 2018, for an overview). Far-field stress influence (e.g. collision between the Indochina and Sibumasu blocks and the terminal closure of Palaeotethys), sudden acceleration of the palaeo-Pacific oceanic plate velocity against the Asian continent, and/or a collapse of an old fracture zone system near the Asian continental margin might have played a major role in spontaneous subduction initiation beneath the SE Asian continental margin at this time. Our study does not allow us to determine unequivocally the cause(s) of subduction initiation beneath East Asia in the latest Palaeozoic – early Mesozoic.

The research done by other geoscientists has shown, however, that active margin tectonics along the SE periphery of continental Asia persisted throughout the Mesozoic Era with changing slab geometry and dip angles (Zhou & Li, 2000; XH Li *et al.* 2006, 2012; Zhou *et al.* 2006; Li & Li, 2007; ZX Li *et al.* 2012; Zhu *et al.* 2013, 2014, 2017; JH Li *et al.* 2018). This convergent margin tectonics produced an intermittently active magmatic arc (ZX Li *et al.* 2012; Duan *et al.* 2018; JH Li *et al.* 2018) and a retroarc foreland basin system with a protracted, complex tectonic history of both extensional and contractional deformation history (Li & Li, 2007; XH Li *et al.* 2012; ZX Li *et al.* 2012, 2014; Pang *et al.* 2014). Permian magmatic arc products are not exposed extensively in SE China, except on Hainan Island where Guadalupian calc-alkaline granites (Wuzhishan granites; *et al.* 2006) exist, and in Anhui Province where Guadalupian volcanic tuff deposits with calc-alkaline geochemistry are well preserved in the Permian sedimentary record (FQ Zhang *et al.* 2020). However, the widespread occurrence of Permian detrital zircons in the Upper Permian through Jurassic sedimentary rock sequences in SE China has been interpreted to have sourced from a magmatic arc in the region (XH Li *et al.* 2012), including the proto-Japan arc (Duan *et al.* 2018; Hara *et al.* 2018; X Zhang *et al.* 2018; Wakita *et al.* 2020).

We infer that an initially large width of the subducting palaeo-Pacific plate against the entire coast of East Asia resulted in flat subduction and resisted slab retreat (Fig. 14a). A global synthesis and three-dimensional modelling of 17 modern subduction zones and their kinematics suggest that the trench-parallel extent of a subducted slab (its width) may vary between 300 and 7000 km, and that it affects the slab dip angle and subduction partitioning along a trench more than the age of the downgoing oceanic lithosphere (Schellart *et al.* 2010; Schellart, 2020). Very large widths of downgoing oceanic plates (8000 to >10 000 km) may resist slab retreat, have fast trench-normal subduction plate velocity and be pushed over by the continental upper plate, causing flat subduction. Conversely, small widths (~1500 km or less) result in slab-buoyancy-driven trench retreat, slow trench-normal subduction plate velocity (and small subduction partitioning – <0.5), and slab steepening with rollback (Schellart *et al.* 2007; Schellart, 2020). The former configuration with flat slab leads into significant crustal shortening in the upper continental plate, as was the case in western North America during the Late Cretaceous – Early Eocene Sevier–Laramide orogeny due to the rapid Farallon plate motion caused by its enormous slab width (>10 000 km; Schellart *et al.* 2010).

Subsequent segmentation of the Farallon plate into a series of smaller plates, such as the Juan de Fuca plate, with significantly reduced widths created slab rollback and upper plate extension during the Neogene (Mooney & Kaban, 2010; YJ Wang *et al.* 2013; Schmandt & Lin, 2014).

Flat subduction of the palaeo-Pacific plate beneath SE China resulted in *push-over tectonics* ($v_4 < v_3 < v_2$ in Fig. 13a), characterized by slow retreat of the subduction hinge and rapid advancement of the continent over the trench. This plate interaction dynamics resulted in strong coupling between the two plates (Fig. 13a). The *push-over* geodynamic scenario caused landward-migrating shortening in the overlying continent and major crustal shortening (>300-km wide in the N–S direction) that manifested in the formation of the *SE China Fold and Thrust Belt* (Fig. 3; JH Li *et al.* 2018). As this flat subduction continued through time, thrust faulting and folding migrated inland (NW) until ~195 Ma. Flat subduction-induced edge flow and asthenospheric uprising (Ballmer *et al.* 2015) led to enriched melts (EMII-type) and the necessary heat to cause partial melting of the lherzolitic subcontinental lithospheric mantle (Fig. 10) and the lower crust to produce high-K granites, syenites and mafic rocks (Fig. 12).

7.b. Slab foundering, trench retreat and upper plate extension

The flat geometry of the subducting palaeo-Pacific oceanic lithosphere for ~50 Ma during the Triassic led to its foundering and delamination, which in turn facilitated the initiation of slab-buoyancy-driven trench retreat and slab steepening in the Early Jurassic (Figs 13b, 14b). Accelerated subduction rate and subduction hinge retreat caused steepening of the downgoing slab, its rapid rollback, and slab segmentation (Fig. 13b). Segmentation of the subducting palaeo-Pacific slab resulted in a major decrease in slab width, which in turn led to *pull-away* subduction dynamics, causing strong decoupling of the upper and lower plates, and then lithospheric-scale extension and magmatism in the upper plate during the Cretaceous (Figs 13c, 14c). Asthenospheric upwelling, replacing the delaminated lower plate, caused metasomatism of the continental mantle lithosphere by OIB-type melts. Partial melting of this modified mantle and the continental crust produced A- and I-type granitoids, syenites with OIB-like geochemical features, and both alkaline and bimodal volcanic rocks (Fig. 11; Yang *et al.* 2018; W Zhang *et al.* 2018; X Zhao *et al.* 2019; this study). Slab-driven trench retreat and slab rollback resulted in upper plate extension, which produced NE–SW-trending, fault-bounded depocentres (grabens), fault-block ranges and metamorphic core complexes (Figs 12, 13b; Lin *et al.* 2008; Wang & Shu, 2012; Li & Li, 2015; JH Li *et al.* 2018; Wang *et al.* 2020). Late Jurassic – Early Cretaceous SE China may have hence resembled the Cenozoic Basin and Range Province in Western North America (Dilek & Moores, 1999; XH Li, 2000; D Wang & Shu, 2012) (see Section 8 for brief discussion of the Basin and Range tectonics and its analogy for Late Jurassic – Early Cretaceous SE China).

7.c. Slab segmentation and steepening, plate decoupling and continental back-arc extension

It has been well demonstrated that changes in rollback velocities along the strike of a subduction zone commonly lead to tearing and segmentation of the subducting lithospheric slab (Govers & Wortel, 2005; Schellart *et al.* 2007; Rosenbaum *et al.* 2008; Dilek & Altunkaynak, 2009). We think that the velocity of subduction rollback along the length of the palaeo-Pacific subduction system

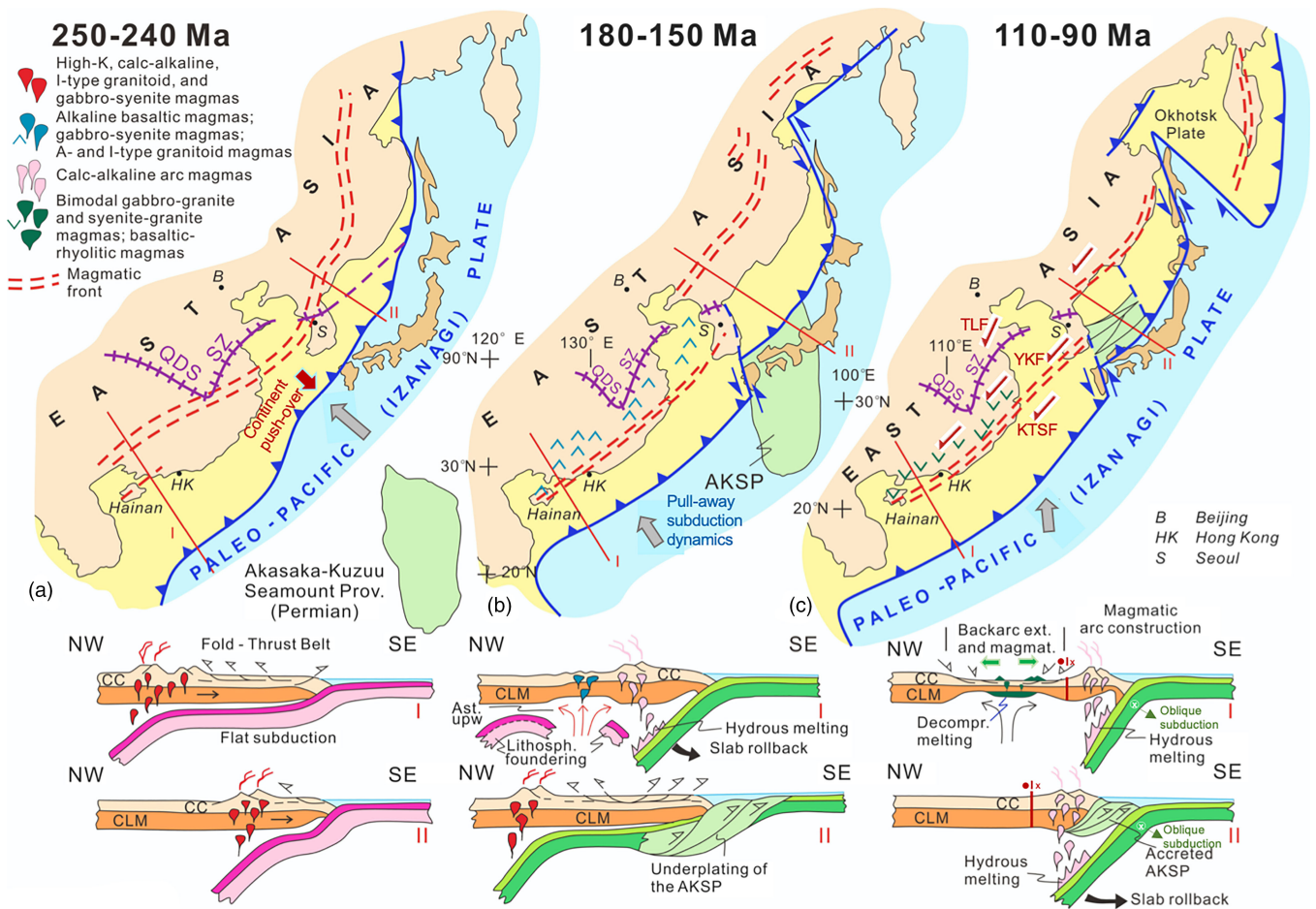


Fig 14. Geodynamic interpretation of subduction-related magmatism and its migration through time and space as a result of the slab geometry of the palaeo-Pacific (Izanagi) oceanic plate and active margin tectonics in East Asia. Broad time windows, keyed into those in Figure 13, include Early to Middle Triassic (250–240 Ma), Jurassic (180–150 Ma) and Albian–Cenomanian (110–90 Ma) in these inferred reconstructions. Outlines of the Japanese archipelago, Sakhalin Island and the Kamchatka Peninsula are provided as reference in these reconstructions. The colour difference on land: buff colour = the Asian continent bounded by the modern shorelines; yellow colour = inferred continental crust along the active continental margin of Asia during Mesozoic times. Lines I and II refer to the tectonic profiles (shown below) across SE China and NE China – SE Russia, respectively. Distributions of major magmatic provinces with their characteristic geochemical affinities are depicted schematically in each reconstruction. QDS – Qinling–Dabie Suture; SZ – Sulu Suture Zone. Major sinistral fault systems that developed inboard of the magmatic arc system during the Late Cretaceous are shown tentatively: KTSF – Korea – Taiwan Strait Fault; TLF – TanLu Fault Zone; YKF – Yongdong–Kwangju Fault. Large grey arrows show the convergence direction of the palaeo-Pacific (Izanagi) oceanic plate with respect to Eurasia. Data are from Faure & Natal'in (1992), Maruyama *et al.* (1997), Lee (1999), WD Sun *et al.* (2007), Hall (2012), ZX Li *et al.* (2012), Wang & Shu (2012), Egawa (2013), Zahirovic *et al.* (2014), Li & Li (2015), YQ Liu *et al.* (2015), SF Liu *et al.* (2017), Tang *et al.* (2018), Zhao *et al.* (2019), Y Zheng *et al.* (2018) and Wakita (2020). See text for discussion of the model.

beneath the Asian continent became varied in time during the Jurassic, resulting in the development of sharp, hairpin-type cusps along its length (Maruyama *et al.* 1997; Li & van der Hilst, 2010; Hall, 2012; Müller *et al.* 2016; SF Liu *et al.* 2017; Zhou & Li, 2017). Furthermore, the arrival of a large oceanic plateau at the palaeo-Pacific subduction trench, such as the Permian Akasaka–Kuzuu Seamount Province (Maruyama *et al.* 1997), likely resulted in significant changes in along-strike slab subduction velocities and in slab tearing (Fig. 14c). Accreted fragments of this seamount province occur in the Kuzu area of Tochigi Prefecture in the central part of Honshu Island in Japan (Kobayashi, 2006). These developments in the palaeo-Pacific subduction dynamics caused slab segmentation and hence decreased slab width. The combination of decreased slab width, continued slab rollback and a more steeply dipping subduction zone in the Cretaceous produced an extended arc-trench and back-arc system in the upper plate (Figs 13c, 14c; Malinovsky *et al.* 2008; J Deng *et al.* 2017; JH Li *et al.* 2018; XY Li *et al.* 2018, 2019).

The southeastward-younging ages of the Cretaceous calc-alkaline rocks in E-SE China are consistent with this slab rollback interpretation. Slab dehydration triggered hydrous melting, which generated arc-like rocks in a magmatic belt close to the coastline (Figs 13c, 14c; Zhou *et al.* 2015). Aesthenospheric decompression melting and low-pressure lower crustal melting beneath the trench-distal back-arc setting formed crustally contaminated MORB-like tholeiitic basalts in an intracontinental extensional system (Fig. 12c; Sun *et al.* 2018; Tang *et al.* 2018).

8. Basin and Range-style extensional tectonics: a recent analogue for Late Jurassic – Early Cretaceous SE China

8.a. Basin and Range tectonics of the Western US Cordillera

The Basin and Range geological province in western North America extends for ~2500 km from Canada in the north, through the Great Basin in the USA, to central Mexico in the south, and

consists of NNW–SSE-oriented, fault-controlled basins (grabens and half-grabens) and mountain ranges (mostly horst blocks). The modern Great Basin is bounded to the west by the Sierra Nevada batholith and mountains in California and the Wasatch mountain range in Utah to the east, and by the Snake River Plain and the Mojave Block in the north and south, respectively. It is a unique physiographic province with a >600 km E–W width, mean elevation of 1500 m a.s.l., average crustal thickness of 30 km and a closed, internal drainage system (Dilek & Moores, 1999). The temperature within its crust and upper mantle is higher than normal, as indicated by the high heat flow and the low seismic velocities in the underlying mantle.

The Basin and Range province behind (or to the east of) the Sierra Nevada magmatic arc was a high plateau with a thick crust (~60 km), supporting high topography (~3 km a.s.l.) in the Late Cretaceous – Palaeogene, after the Cordilleran orogeny (Dilek & Moores, 1999; Liu, 2001; Best *et al.* 2009). Saline lakes were developed on this altiplano in the Eocene, reminiscent of today's Tibetan plateau north of the Himalaya Mountains (Dilek & Moores, 1999). The Late Cretaceous – Palaeogene Laramide magmatism, which was associated with the flat Farallon slab, migrated eastward across the Great Basin (Dickinson, 2006). However, by the Late Eocene – Oligocene the unusually thick crust and high topography of the Great Basin became unstable as the excess gravitational potential energy, thermal relaxation and enhanced radiogenic heating caused partial melting in the middle to lower crust that in turn resulted in the onset of orogenic collapse and extensional deformation (Liu, 2001). This orogenic collapse also overlapped in time and space with re-migration of magmatism westwards across the Great Basin and towards the continental margin, as the segmented Farallon plate started dipping more steeply below the North American continent (Atwater & Stock, 1998; Dickinson, 2006; Schellart *et al.* 2010; Wang *et al.* 2012). Aesthenospheric upwelling associated with the steeply dipping and fast-retreating, narrow Farallon slabs provided the necessary heat source for extensive crustal melting and induced thermal weakening, which collectively led to significant extensional deformation, crustal exhumation, and denudation of crystalline basement rocks forming metamorphic core complexes in the Great Basin during the Oligo-Miocene (Dilek & Moores, 1999; Dickinson, 2006).

The Late Tertiary metamorphic core complexes in western North America are situated in the hinterland of the Late Jurassic – Early Eocene Sevier fold-and-thrust belt (Taylor *et al.* 2000), and stretch from the British Columbia (Canada) latitude in the north, through the Great Basin in the USA, to the Sonora Desert in northern Mexico. They are characterized by dome-shaped, highly deformed metamorphic and magmatic rocks in the footwalls of low-angle detachment faults, overlain by undeformed, terrestrial clastic rocks deposited in supradetachment basins and structural grabens. The exhumation of these metamorphic core complexes was synchronous with widespread outburst of commonly caldera-centred ignimbrite eruptions (Dilek & Moores, 1999). The 'ignimbrite flare-up' episode was coeval with the emplacement of metaluminous to mildly peraluminous granitoid plutons at depth and voluminous eruptions of rhyolitic, rhyodacitic ash-flow tuffs and high-K dacitic to andesitic lava flows (Best *et al.* 2009; Henry & John, 2013). This volcanic phase was temporally associated with thin-skinned extensional deformation across the Great Basin that produced closely spaced, high-angle and shallow listric normal faults, and fault-bounded and strongly tilted stratigraphic–volcanic sequences (Proffett, 1977; Lipman,

1984; Johnson *et al.* 1989; Bachl *et al.* 2001). All these tectonic and magmatic events were largely a result of back-arc extension in the western North American Cordillera during the Mid-Cenozoic.

A second phase of the Basin and Range extension started around 18–16 Ma and developed block-faulting, regional subsidence and bimodal basaltic–rhyolitic volcanism (Dilek & Moores, 1999; Best *et al.* 2009). Eruption of alkaline basaltic lavas during this phase indicates the involvement of SCLM in the melt evolution. Strike-slip faulting in the western end of the Great Basin later in the Miocene shows that the mode of extensional deformation was largely controlled by transtension, rather than back-arc extension, as the San Andreas transform fault system replaced the active margin tectonics along the Pacific – North American plates (Atwater & Stock, 1998). Strain partitioning along and across the San Andreas transform fault system produced a series of NNW–SSE-striking, dextral transtensional fault systems (i.e. the Walker Lane Shear Zone), which have been accommodating ~25–15% of the Pacific – North American plate motion (Faulds *et al.* 2005) and facilitating the N–NW motion of the Sierran – Great Valley block with respect to the Colorado Plateau (fixed North American plate) at an average rate of 15 mm a⁻¹ since 10–8 Ma (Wernicke & Snow, 1998).

8.b. Basin and Range analogue for Late Jurassic – Cretaceous SE China

There are many similarities between the Cenozoic geology and tectonics of the Western US Cordillera and the Late Jurassic – Cretaceous geology and tectonics of SE China, suggesting that similar geodynamic processes may have controlled their continental dynamics, specifically their tectonomagmatic and landscape evolution. Here, we draw some first-order parallels between these two continental regions, regarding the nature of major geological events and their consequences in a relative time frame.

- (1) Both the Western US Cordillera and SE China experienced flat-slab subduction of oceanic plates against their continental margins that resulted in contractional deformation, which migrated inland through time.
- (2) The onset of the following extensional deformation and attendant magmatism in both continental regions was associated with more steeply dipping and retreating oceanic slabs. It is inferred that this slab dynamics was a result of slab segmentation and hence major reduction in the widths of subducting slabs. Coeval magmatism migrated across the continental upper plates, towards the active margins, and produced bimodal volcanic rocks and granitoid intrusions, some of which resulted from partial melting of continental lower crust. This magmatism caused thermal weakening of the continental crust.
- (3) Thermally weakened continental crust in the back-arc tectonic setting in both the Western US Cordillera and SE China subsequently underwent crustal exhumation and denudation of crystalline basement rocks. This process led to the development of metamorphic core complexes in the footwalls of low-angle detachment faults, which were overlapped by syn-extensional and terrestrial, supradetachment depocentres. This tectonic episode was also synchronous with the development of playa lakes within basins, separated by ranges, representing uplifted fault blocks. The landscape evolution in both regions was a manifestation of thin-skinned tectonics, with

extensive alluvial fan system and internal drainage formation, and deposition of evaporites and lacustrine sediments.

- (4) Spatially and temporally overlapped with metamorphic core complex formation was widespread eruption of rhyolitic, dacitic and andesitic tuffs and production of ignimbrites and ashfall deposits. In both SE China and in the Great Basin of the Western US Cordillera this unique magmatic event is known as ‘*ignimbrite flare-up*’, which was associated with the emplacement of shallow-level granitic plutons.
- (5) Later-stage extensional deformation involved block-faulting, regional subsidence and bimodal (basaltic–rhyolitic) volcanism in both SE China and the Great Basin. Basaltic magmatism was a result of aesthenospheric decompression melting beneath significantly thinned continental lithosphere, and was locally fed by mafic dyke swarms, which were emplaced perpendicular to the regional tensile stress regimes.
- (6) With the convergence direction of the subducting plates becoming more oblique with respect to the active margins of E-SE China and the Western US Cordillera through time, oblique subduction and the associated strain partitioning in the upper continental plates resulted in transtensional deformation. Major strike-slip fault systems developed, such as the Tanlu Fault in East China (Y Zhang *et al.* 2020) and the Walker Lane shear zone in western Nevada and eastern California (Faulds *et al.* 2005), which strongly affected the crustal architecture of the continental margins in both regions.

This comparative summary shows that the time-progressive tectonic, magmatic and landscape evolution of Mesozoic SE China and the Cenozoic Western US Cordillera followed similar tectonic paths through time while undergoing similar geodynamic events. Although these two regions had significantly different geodynamic histories prior to the onset of flat-slab subduction along their continental margins, their SCLM and continental crust responded to the subducting slab dynamics and changing slab geometries in similar ways.

9. Conclusions

The geochemical fingerprints of magmatic rocks and the tectonic architecture of the continental crust on Hainan and in SE China in general were strongly affected by the motions of subducting plates and trench migration through time. A nearly complete record of the Triassic through Cretaceous igneous events, as discussed in this study, points to progressive melt evolution from alkaline through tholeiitic and OIB type, to magmas with calc-alkaline affinities, reflecting the changing character of the mantle source and slab dynamics beneath E-SE China. This magmatic progression overlapped with and followed a major tectonic switch from contractional deformation in the Triassic to lithospheric-scale extensional deformation during the Jurassic and Cretaceous. Our geodynamic model envisions a mode switch from a Laramide-type, flat-slab controlled contractional to a moderately-to-steeply dipping palaeo-Pacific slab geometry and Basin and Range-type extensional tectonics, reminiscent of the Late Cretaceous – Cenozoic North American Cordillera (Dilek & Moores, 1999; Dickinson, 2006; Wells *et al.* 2012, and references therein). This ‘push–pull geodynamics’ of Mesozoic E-SE China occurred during ~150 Ma of continuous convergence between the continental China and the oceanic palaeo-Pacific plate. Slab segmentation and fragmentation, which reduced the along-strike width of the subducting palaeo-Pacific plate, played a major role in the steepening and

retreat of the downgoing oceanic slabs that in turn induced aesthenospheric upwelling, increasingly more mafic magmatism and lithospheric-scale thinning in the continental upper plate during the Middle Jurassic through Cretaceous.

The geology of Mesozoic E-SE China is a great natural laboratory to investigate the slab-controlled continental dynamics through time. Further systematic, precise geochronological and structural field studies of the Jurassic and Cretaceous magmatic rock suites, terrestrial basin deposits and extensional and strike-slip fault systems in SE China should further elucidate the validity of our analogy of its Basin and Range-type tectonic evolution during the Middle to Late Mesozoic.

Acknowledgements. Our fieldwork on Hainan Island was supported by research funds from the Second Institute of Oceanography to LM Tang. Y Dilek acknowledges field support by Zhejiang University for his research on Hainan Island. Formal reviews for the *Geological Magazine* by M Faure and WJ Xiao have helped us refine our interpretations and the model presented in this paper. Constructive and insightful reviews by Y Ogawa and Editor P Clift are gratefully acknowledged. We thank Susie (Bloor) Cox for her continued help and support, and Editor Peter Clift for his objective and constructive editorial handling of our paper.

Conflict of interest. None.

Supplementary material. To view supplementary material for this article, please visit <https://doi.org/10.1017/S0016756820001211>

References

- Ai YS, Chen QF, Zeng F, Hong X and Ye WY (2007) The crust and upper mantle structure beneath southeastern China. *Earth and Planetary Science Letters* **260**, 549–63.
- Aldanmaz E, Pearce JA, Thirlwall MF and Mitchell JG (2000) Petrogenetic evolution of late Cenozoic, post-collision volcanism in western Anatolia, Turkey. *Journal of Volcanology and Geothermal Research* **102**, 67–95.
- Atwater T and Stock J (1998) Pacific–North America plate tectonics of the Neogene south southwestern United States: an update. *International Geology Review* **40**, 375–402.
- Bachl CA, Miller CF, Miller JS and Faulds JE (2001) Construction of a pluton: evidence from an exposed cross section of the Searchlight pluton, Eldorado Mountains, Nevada. *Geological Society of America Bulletin* **113**, 1213–28.
- Ballmer MD, Conrad CP, Smith EI and Johnsen R (2015) Intraplate volcanism at the edges of the Colorado Plateau sustained by a combination of triggered edge-driven convection and shear-driven upwelling. *Geochemistry, Geophysics, Geosystems* **16**. doi: [10.1002/2014GC005641](https://doi.org/10.1002/2014GC005641).
- Best MG, Barr DL, Christiansen EH, Gromme S, Deino AL and Tingey DG (2009) The Great Basin Altiplano during the middle Cenozoic ignimbrite flareup: insights from volcanic rocks. *International Geology Review* **51**, 589–633. doi: [10.1080/00206810902867690](https://doi.org/10.1080/00206810902867690).
- Boynton WV (1984) Geochemistry of the rare earth elements: meteorite studies. In *Rare Earth Element Geochemistry* (ed P. Henderson), pp. 63–114. Amsterdam: Elsevier/rtorp.
- Byrne T, Chan YC, Rau RJ, Lu CY, Lee YH and Wang YJ (2011) The arc-continent collision in Taiwan. In *Arc-Continent Collision, Frontiers in Earth Sciences* (eds D Brown and PD Ryan), pp. 213–45. Berlin/Heidelberg: Springer-Verlag. doi: [10.1007/978-3-540-88558-0_8](https://doi.org/10.1007/978-3-540-88558-0_8).
- Carter A and Clift PD (2008) Was the Indosinian orogeny a Triassic mountain building or a thermotectonic reactivation event? *Comptes Rendus Geoscience* **340**, 83–93. doi: [10.1016/j.crte.2007.08.011](https://doi.org/10.1016/j.crte.2007.08.011).
- Charvet J, Shu LS, Shi YS, Guo LZ and Faure M (1996) The building of south China: collision of Yangtze and Cathaysia Blocks, problems and tentative answers. *Journal of Southeast Asian Earth Sciences* **13**, 223–35.
- Chen WH, Huang CY, Yan Y, Dilek Y, Chen D, Wang MH, Zhang X, Lan Q and Yu M (2017) Stratigraphy and provenance of forearc sequences in the Lichi Mélange, Coastal Range: geological records of the active Taiwan arc-

- continent collision. *Journal of Geophysical Research – Solid Earth* **122**, 7408–36. doi: [10.1002/2017JB014378](https://doi.org/10.1002/2017JB014378).
- Chu Y, Faure M, Lin W, Wang QC and Ji W-B** (2012) Tectonics of the Middle Triassic intracontinental Xuefengshan Belt, South China: new insights from structural and chronological constraints on the basal décollement zone. *International Journal of Earth Sciences* **101**, 2125–50.
- Chu Y, Lin W, Faure M, Xue Z, Ji W and Feng Z** (2019) Cretaceous episodic extension in the South China Block, East Asia: evidence from the Yuechengling Massif of central South China. *Tectonics* **38**. doi: [10.1029/2019TC005516](https://doi.org/10.1029/2019TC005516).
- Deng J, Liu XF, Wang QF, Dilek Y and Liang Y** (2017) Isotopic characterization and petrogenetic modeling of early Cretaceous mafic dike – lithospheric extension in the North China Craton, Eastern Asia. *Geological Society of America Bulletin* **129**, 1379–407. doi: [10.1130/B31609.1](https://doi.org/10.1130/B31609.1).
- Dickinson WR** (2006) Geotectonic evolution of the Great Basin. *Geosphere* **2**, 353–68. doi: [10.1130/GES00054.1](https://doi.org/10.1130/GES00054.1).
- Dilek Y** (2006) Collision tectonics of the Mediterranean region: causes and consequences. In *Postcollisional Tectonics and Magmatism in the Mediterranean Region and Asia* (eds Y Dilek and S Pavlides), pp. 1–13. Geological Society of America Special Paper 409. doi: [10.1130/2006.2409\(01\)](https://doi.org/10.1130/2006.2409(01)).
- Dilek Y and Altunkaynak Ş** (2009) Geochemical and temporal evolution of Cenozoic magmatism in western Turkey: mantle response to collision, slab break-off, and lithospheric tearing in an orogenic belt. In *Collision and Collapse of the Africa-Arabia-Eurasia Subduction Zone* (eds DJJ van Hinsbergen, MA Edwards and R Govers), pp. 213–33. Geological Society of London, Special Publication no. 311.
- Dilek Y and Furnes H** (2009) Structure and geochemistry of Tethyan ophiolites and their petrogenesis in subduction rollback systems. *Lithos* **113**, 1–20. doi: [10.1016/j.lithos.2009.04.022](https://doi.org/10.1016/j.lithos.2009.04.022).
- Dilek Y and Furnes H** (2011) Ophiolite genesis and global tectonics: geochemical and tectonic fingerprinting of ancient oceanic lithosphere. *Geological Society of America Bulletin* **123**, 387–411. doi: [10.1130/B30446.1](https://doi.org/10.1130/B30446.1).
- Dilek Y and Furnes H** (2014) Origins of ophiolites. *Elements* **10**, 93–100. doi: [10.2013/gselements.10.2.93](https://doi.org/10.2013/gselements.10.2.93).
- Dilek Y, Imamverdiyev N and Altunkaynak Ş**, 2010, Geochemistry and tectonics of Cenozoic volcanism in the Lesser Caucasus (Azerbaijan) and the peri-Arabian region: collision-induced mantle dynamics and its magmatic fingerprint. *International Geology Review* **52**, 536–78. doi: [10.1080/00206810903360422](https://doi.org/10.1080/00206810903360422).
- Dilek Y and Moores EM** (1999) A Tibetan model for the early Tertiary western United States. *Journal of the Geological Society* **156**, 929–41. doi: [10.1144/gsjgs.156.5.0929](https://doi.org/10.1144/gsjgs.156.5.0929).
- Dilek Y and Whitney DL** (2000) Cenozoic crustal evolution in Central Anatolia: extension, magmatism and landscape development. In *Proceedings of the Third International Conference on the Geology of the Eastern Mediterranean* (eds I Panayides, C Xenophontos and J Malpas), pp. 183–92. Nicosia, Cyprus: Geological Survey Department.
- Ding DG, Guo TL, Liu YL and Zhai CB** (2007) Structural attribute of the Jiangnan–Xuefengshan belt, China: a discussion. *Geological Bulletin of China* **26**, 801–9 (in Chinese with English abstract).
- Domeier M and Torsvik TH** (2014) Plate tectonics in the late Paleozoic. *Geoscience Frontiers* **5**, 303–50. doi: [10.1016/j.gsf.2014.01.002](https://doi.org/10.1016/j.gsf.2014.01.002).
- Dong M, Wu SG, Zhang J, Xu X, Gao JW and Song T** (2018) Lithospheric structure of the Southwest South China Sea: implications for rifting and extension. *International Geology Review* **62**. doi: [10.1080/00206814.2018.1539926](https://doi.org/10.1080/00206814.2018.1539926).
- Duan L, Meng QR, Christie-Blick N and Wu GL** (2018) New insights on the Triassic tectonic development of South China from the detrital zircon provenance of Nanpanjiang turbidites. *Geological Society of America Bulletin* **130**, 24–34. doi: [10.1130/B31630.1](https://doi.org/10.1130/B31630.1).
- Egawa K** (2013) East Asia-wide flat slab subduction and Jurassic synorogenic basin evolution in West Korea. In *Mechanism of Sedimentary Basin Formation – Multidisciplinary Approach on Active Plate Margins* (ed. Y Itoh), pp. 61–81. IntechOpen. doi: [10.5772/56770](https://doi.org/10.5772/56770).
- Escrig S, Capmas F, Dupre' B and Allegre CJ** (2004) Osmium isotopic constraints on the nature of the DUPAL anomaly from Indian mid-ocean-ridge basalts. *Nature* **431**, 59–63. doi: [10.1038/nature02904](https://doi.org/10.1038/nature02904).
- Faulds JE, Henry CD and Hinz NH** (2005) Kinematics of the northern Walker Lane: an incipient transform fault along the Pacific–North American plate boundary. *Geology* **33**, 505–8. doi: [10.1130/G21274.1](https://doi.org/10.1130/G21274.1).
- Faure M, Lepvrier C, Nguyen VV, Vu TV, Lin W and Chen Z** (2014) The South China block–Indochina collision: where, when, and how? *Journal of Asian Earth Sciences* **79**, 260–74.
- Faure M, Lin W, Chu Y and Lepvrier C** (2016) Triassic tectonics of the southern margin of the South China Block. *Comptes Rendus Geoscience* **348**, 5–14.
- Faure M, Lin W, Monié P and Meffre S** (2008) Palaeozoic collision between the North and South China blocks, Triassic intracontinental tectonics, and the problem of the ultrahigh-pressure metamorphism. *Comptes Rendus Geoscience* **340**, 139–50.
- Faure M and Natal'in B** (1992) The geodynamic evolution of the eastern Eurasian margin in Mesozoic times. *Tectonophysics* **208**, 397–411.
- Faure M, Shu LS, Wang B, Charvet J, Choulet F and Monié P** (2009) Intracontinental subduction: a possible mechanism for the Early Paleozoic orogen of SE China. *Terra Nova*. doi: [10.1111/j.1365-3121.2009.00888](https://doi.org/10.1111/j.1365-3121.2009.00888).
- Faure M, Sun Y, Shu L, Monié P and Charvet J** (1996) Extensional tectonics within a subduction-type orogen. The case study of the Wugongshan dome (Jiangxi Province, southeastern China). *Tectonophysics* **263**, 77–106.
- Gao W, Wang ZX, Li L and Tan YL** (2019a) Petrogenesis and tectonic implications of Triassic A-type granites in southeastern China: insights from zircon U–Pb–Hf isotopic and whole-rock geochemical compositions of the Luoguyan and Guiyuantou granites in northwestern Fujian Province. *International Geology Review* **61**, 224–39. doi: [10.1080/00206814.2017.1422444](https://doi.org/10.1080/00206814.2017.1422444).
- Gao WL, Wang ZX, Tan YL and Li LL** (2019b) Zircon U–Pb–Hf isotopic and trace-element geochemistry constraints on the Late Jurassic–Early Cretaceous magmatic evolution of Southeastern Zhejiang, South China. *Journal of Geology* **127**, 363–79. doi: [10.1086/702624](https://doi.org/10.1086/702624).
- Ge XY** (2003) *Mesozoic magmatism in Hainan Island (SE China) and its tectonic significance: geochronology, geochemistry and Sr–Nd isotope evidences*. PhD thesis, Guangzhou Institute of Geochemistry, Chinese Academy of Science, Guanzhou, China, 87 pp.
- Geng HY, Xu X, O'Reilly SY, Zhao M and Sun T** (2006) Cretaceous volcanic-intrusive magmatism in western Guangdong and its geological significance. *Science China, Series D* **49**, 696–713. doi: [10.1007/s11430-006-0696-7](https://doi.org/10.1007/s11430-006-0696-7).
- Govers R and Wortel MJR** (2005) Lithosphere tearing at STEP faults: response to edges of subduction zones. *Earth Planetary Science Letters* **236**, 505–23. doi: [10.1016/j.epsl.2005.03.022](https://doi.org/10.1016/j.epsl.2005.03.022).
- Guo C, Chen Y, Zeng Z and Lou F** (2012) Petrogenesis of the Xihuashan granites in southeastern China: constraints from geochemistry and in-situ analyses of zircon U–Pb–Hf–O isotopes. *Lithos* **148**, 209–27. doi: [10.1016/j.lithos.2012.06.014](https://doi.org/10.1016/j.lithos.2012.06.014).
- Guo F, Fan WM, Li C, Zhao L, Li H and Yang JH** (2012) Multi-stage crust–mantle interaction in SE China: temporal, thermal and compositional constraints from the Mesozoic felsic volcanic rocks in eastern Guangdong–Fujian provinces. *Lithos* **150**, 62–84. doi: [10.1016/j.lithos.2011.12.009](https://doi.org/10.1016/j.lithos.2011.12.009).
- Hall R** (2012) Late Jurassic–Cenozoic reconstructions of the Indonesian region and the Indian Ocean. *Tectonophysics* **570–571**, 1–41. doi: [10.1016/j.tecto.2012.04.021](https://doi.org/10.1016/j.tecto.2012.04.021).
- Hara H, Hirano M, Kurihara T, Takahashi T and Ueda H**, 2018, Permian arc evolution associated with Panthalassa subduction along the eastern margin of the south China block, based on sandstone provenance and U–Pb detrital zircon ages of the Kurosegawa belt, southwest Japan. *Journal of Asian Earth Sciences* **151**, 112–30. doi: [10.1016/j.jseaes.2017.10.025](https://doi.org/10.1016/j.jseaes.2017.10.025).
- He CS, Dong S, Santosh M and Chen XH** (2013) Seismic evidence for a geosuture between the Yangtze and Cathaysia Blocks, South China. *Nature Scientific Reports* **3**, 2200. doi: [10.1038/srep02200](https://doi.org/10.1038/srep02200).
- He ZY, Xu XS and Niu YL** (2010) Petrogenesis and tectonic significance of a Mesozoic granite–syenite–gabbro association from inland South China. *Lithos* **119**, 621–41.
- Henry CD and John DA** (2013) Magmatism, ash-flow tuffs, and calderas of the ignimbrite flareup in the western Nevada volcanic field, Great Basin, USA. *Geosphere* **9**, 951–1008.
- Hu L, Cawood PA, Du YS, Xu Y, Wang C, Wang Z, Ma Q and Xu X** (2017) Permo-Triassic detrital records of South China and implications for the

- Indosinian events in East Asia. *Palaeogeography, Palaeoclimatology, Palaeoecology* **485**, 84–100. doi: [10.1016/j.palaeo.2017.06.005](https://doi.org/10.1016/j.palaeo.2017.06.005).
- Hu Y, Hao M, Jia L and Song SW (2016) Three-dimensional crustal movement and the activities of earthquakes, volcanoes and faults in Hainan Island, China. *Geodesy and Geodynamics* **17**, 284–94.
- Huang GP, Wang P, Yu M, You CF, Liu CS, Zhao X, Shao L, Zhong G and Yumul GJ Jr (2019) Potential role of strike-slip faults in opening up the South China Sea. *National Science Review* **6**, 891–901. doi: [10.1093/nsr/nwz119](https://doi.org/10.1093/nsr/nwz119).
- Jamali H, Dilek Y, Daliran F, Yaghubpur A and Mehrabi B (2010) Metallogeny and tectonic evolution of the Cenozoic Ahar–Arasbaran volcanic belt, northern Iran. *International Geology Review* **52**, 608–630.
- Ji W, Lin W, Faure M, Chen Y, Chu Y and Xue ZH (2017) Origin of the Late Jurassic to Early Cretaceous peraluminous granitoids in the northeastern Hunan province (middle Yangtze region), South China: geodynamic implications for the Paleo-Pacific subduction. *Journal of Asian Earth Sciences* **141**, 74–193.
- Jiang YH, Jiang SY, Zhao KD and Ling HF (2006) Petrogenesis of Late Jurassic Qianlishan granites and mafic dykes, Southeast China: implications for a back-arc extension setting. *Geological Magazine* **143**, 457–74.
- Johnson CM, Shannon JR and Fridrich CJ (1989) Roots of ignimbrite calderas: batholithic plutonism, volcanism, and mineralization in the Southern Rocky Mountains, Colorado and New Mexico. In *Field Excursions to Volcanic Terrains in the Western United States, Volume I: Southern Rocky Mountains Region* (eds CE Chapin and J Zidek). New Mexico Bureau of Mines and Mineral Resources, 46, 275–302.
- Kobayashi F (2006) Middle Permian foraminifers of the Izuru and Nabeyama Formations in the Kuzu area, Tochigi Prefecture, Japan Part 1. Schwagerinid, neoschwagerinid, and verbeekiniid fusulinoideans. *Paleontological Research* **10**, 37–59.
- Lapierre H, Jahn BM, Charvet J and Yu YW (1997) Mesozoic felsic arc magmatism and continental olivine tholeiites in Zhejiang Province and their relationship with the tectonic activity in southeastern China. *Tectonophysics* **274**, 321–38. doi: [10.1016/S0040-1951\(97\)00009-7](https://doi.org/10.1016/S0040-1951(97)00009-7).
- Le Bas MJ, Le Maitre RW and Streckelsen A (1986) A chemical classification of volcanic rocks based on the total alkali-silica diagram. *Journal of Petrology* **27**, 745–50. doi: [10.1093/petrology/27.3.745](https://doi.org/10.1093/petrology/27.3.745).
- Lee DW (1999) Strike-slip fault tectonics and basin formation during the Cretaceous in the Korean Peninsula. *Island Arc* **8**, 218–31.
- Li C and van der Hilst RD (2010) Structure of the upper mantle and transition zone beneath Southeast Asia from traveltimes tomography. *Journal of Geophysical Research* **115**, B07308. doi: [10.1029/2009JB006882](https://doi.org/10.1029/2009JB006882).
- Li J, Dong S, Zhang Y, Zhao G, Johnston ST, Cui J and Xin Y (2016) New insights into Phanerozoic tectonics of south China: Part 1, polyphase deformation in the Jiuling and Lianyunshan domains of the central Jiangnan Orogen. *Journal of Geophysical Research – Solid Earth* **121**. doi: [10.1002/2015JB012778](https://doi.org/10.1002/2015JB012778).
- Li J, Zhang Y, Dong S and Johnston ST (2014) Cretaceous tectonic evolution of South China: a preliminary synthesis. *Earth-Science Reviews* **134**, 98–136. doi: [10.1016/j.earscirev.2014.03.008](https://doi.org/10.1016/j.earscirev.2014.03.008).
- Li JH, Dong S, Cawood PA, Zhao G, Johnson ST, Zhang Y and Xin Y (2018) An Andean-type retro-arc foreland system beneath northwest South China revealed by SINOPROBE profiling. *Earth and Planetary Science Letters* **490**, 170–9.
- Li JH, Zhang Y, Zhao G, Johnston ST, Dong SW, Koppers A, Miggins DP, Sun H, Wang W and Xin Y (2017) New insights into Phanerozoic tectonics of South China: Early Paleozoic sinistral and Triassic dextral transpression in the east Wuyishan and Chencai domains, NE Cathaysia. *Tectonics* **36**, 819–53. doi: [10.1002/2016TC004461](https://doi.org/10.1002/2016TC004461).
- Li PJ and Li HY (2015) Geochronological, sedimentary, structural, and metallogenic characteristics of southeast China during the Mesozoic: a general review. *International Journal of Geosciences* **6**, 1032–47.
- Li Q, Gao R, Wu FT, Guan Y, Ye Z, Liu Q, Hao KC, He R, Li W and Shen X (2013) Seismic structure in the southeastern China using teleseismic receiver functions. *Tectonophysics* **606**, 24–35.
- Li XH (2000) Cretaceous magmatism and lithosphere extension in southeast China. *Journal of Asian Earth Sciences* **18**, 293–305.
- Li XH, Chen Z, Liu D and Li WX (2003) Jurassic gabbro-granite-syenite suites from southern Jiangxi Province, SE China: age, origin, and tectonic significance. *International Geology Review* **45**, 898–921.
- Li XH, Li ZX, He B, Li WX, Li QL, Gao YY and Wang XC (2012) The Early Permian active continental margin and crustal growth of the Cathaysia Block: in situ U–Pb, Lu–Hf and O isotope analyses of detrital zircons. *Chemical Geology* **328**, 195–207. doi: [10.1016/j.chemgeo.2011.10.027](https://doi.org/10.1016/j.chemgeo.2011.10.027).
- Li XH, Li ZX, Li WX and Wang Y (2006) Initiation of the Indosinian Orogeny in South China: evidence for a Permian magmatic arc on Hainan Island. *Journal of Geology* **114**, 341–53. doi: [10.1086/501222](https://doi.org/10.1086/501222).
- Li XH and McCulloch MT (1998). Geochemical characteristics of Cretaceous mafic dikes from northern Guangdong, SE China: age, origin and tectonic significance. In *Mantle Dynamics and Plate Interaction in East Asia* (eds MFJ Flower, SL Chung, CH Lo and TY Lee), American Geophysical Union Geodynamics Series, No. 27, pp. 405–19.
- Li XY, Zhou HW, Chung SL, Ding S, Liu Y, Lee CY, Ge W, Zhang Y and Zhang R (2002) Geochemical and Sm–Nd isotopic characteristics of metabasites from central Hainan Island, South China and their tectonic significance. *Island Arc* **11**, 193–205.
- Li XY, Li S, Huang F, Wang Y, Yu S, Cao H and Xie W (2019) Petrogenesis of high Ba–Sr plutons with high Sr/Y ratios in an intracontinental setting: evidence from Early Cretaceous Fushan monzonites, central North China Craton. *Geological Magazine* **156**, 1965–81. doi: [10.1017/S0016756819000256](https://doi.org/10.1017/S0016756819000256).
- Li XY, Li SZ, Suo YH, Dai LM, Guo LL, Ge FJ and Lin PP (2018) Late Cretaceous basalts and rhyolites from Shimaoshan Group in eastern Fujian Province, SE China: age, petrogenesis, and tectonic implications. *International Geology Review* **60**, 1721–43. doi: [10.1080/00206814.2017.1353447](https://doi.org/10.1080/00206814.2017.1353447).
- Li Z, Qiu JS and Xu XS (2012) Geochronological, geochemical and Sr–Nd–Hf isotopic constraints on petrogenesis of Late Mesozoic gabbro–granite complexes on the southeast coast of Fujian, South China: insights into a depleted mantle source region and crust–mantle interactions. *Geological Magazine* **149**, 459–82.
- Li ZX and Li XH (2007) Formation of the 1300 km wide intracontinental orogen and postorogenic magmatic province in Mesozoic South China: a flat-slab subduction model. *Geology* **35**, 179–82.
- Li ZX, Li XH, Chung SL, Lo CH, Xu X and Li WX (2012) Magmatic switch-on and switch-off along the South China continental margin since the Permian: transition from an Andean-type to a Western Pacific-type plate boundary. *Tectonophysics* **532–535**, 271–90.
- Li ZX, Li XH, Wartho JA, Clark C, Li WX, Zhang CL and Bao C (2010) Magmatic and metamorphic events during the Early Paleozoic Wuyi–Yunkai orogeny, south-eastern South China: new age constraints and pressure–temperature conditions. *Geological Society of America Bulletin* **122**, 772–93.
- Lin S, Xing GF, Davis DW, Yin CQ, Wu ML, Li LM, Jiang Y and Chen ZH (2018) Appalachian-style multi-terrane Wilson cycle model for the assembly of South China. *Geology* **46**, 319–22.
- Lin W, Faure M, Monié P, Schärer U and Panis D (2008) Mesozoic extensional tectonics in Eastern Asia: the South Liaodong Peninsula metamorphic core complex (NE China). *Journal of Geology* **116**, 134–54. doi: [10.1086/527456](https://doi.org/10.1086/527456).
- Lin W and Wang QC. (2006) Late Mesozoic extensional tectonics in the North China block: a crustal response to subcontinental mantle removal? *Bulletin de la Société Géologique de France* **177**, 287–97.
- Lipman PW (1984) The roots of ash-flow calderas in western North America: windows into the tops of granitic batholiths. *Journal of Geophysical Research* **89**, 8801–41.
- Lister G and Foster M (2009) Tectonic mode switches and the nature of orogenesis. *Lithos* **113**, 274–91.
- Liu CZ, Wu FW, Sun J, Chu ZY and Qiu ZQ (2012) The Xinchang peridotite xenoliths reveal mantle replacement and accretion in southeastern China. *Lithos* **150**, 171–87. doi: [10.1016/j.lithos.2012.03.019](https://doi.org/10.1016/j.lithos.2012.03.019).
- Liu CZ, Zhang C, Liu ZC, Sun J, Chu ZY, Qiu ZL and Wu FY (2017) Formation age and metasomatism of the sub-continental lithospheric mantle beneath Southeast China: Sr–Nd–Hf–Os isotopes of Mingxi mantle xenoliths. *Journal of Asian Earth Sciences* **145**, 591–604. doi: [10.1016/j.jseaes.2017.06.013](https://doi.org/10.1016/j.jseaes.2017.06.013).
- Liu K, Zhang JJ, Wilde SA, Zhou J, Wang M, Ge MH, Wang JM and Ling YY (2017) Initial subduction of the Paleo-Pacific Oceanic plate in NE China: constraints from whole-rock geochemistry and zircon U–Pb and Lu–Hf isotopes of the Khanka Lake granitoids. *Lithos* **274–275**, 254–70.

- Liu L, Qiu J, Zhao JL and Yang ZL** (2014) Geochronological, geochemical, and Sr–Nd–Hf isotopic characteristics of Cretaceous monzonitic plutons in western Zhejiang Province, Southeast China: new insights into the petrogenesis of intermediate rocks. *Lithos* **196–197**, 242–60. doi: [10.1016/j.lithos.2014.03.010](https://doi.org/10.1016/j.lithos.2014.03.010).
- Liu M** (2001) Cenozoic extension and magmatism in the North American Cordillera: the role of gravitational collapse. *Tectonophysics* **342**, 407–33.
- Liu S, Zou H, Hu R, Zhao J and Feng C** (2006) Mesozoic mafic dikes from the Shandong Peninsula, North China Craton: petrogenesis and tectonic implications. *Geochemical Journal* **40**, 181–95.
- Liu SF, Gurnis M, Ma PF and Zhang B** (2017) Reconstruction of northeast Asian deformation integrated with western Pacific plate subduction since 200 Ma. *Earth Science Reviews* **175**, 114–42. doi: [10.1016/j.earscirev.2017.10.012](https://doi.org/10.1016/j.earscirev.2017.10.012).
- Liu YQ, Kuang HW, Peng N, Xu H, Zhang P, Wang NS and An W** (2015) Mesozoic basins and associated palaeogeographic evolution in North China. *Journal of Palaeogeography* **4**, 189–202.
- Ma H, Wang Y, Huang Y and Xie Y** (2019) Three-stage Mesozoic intracontinental tectonic evolution of South China recorded in an overprinted basin: evidence from stratigraphy and detrital zircon U–Pb dating. *Geological Magazine* **156**, 2085–103. doi: [10.1017/S00167568190006451](https://doi.org/10.1017/S00167568190006451).
- Malavieille J, Dominguez S, Lu CY, Chen CT and Konstantinovskaya E** (2020) Deformation partitioning in mountain belts: insights from analogue modelling experiments and the Taiwan collisional orogen. *Geological Magazine*, doi: [10.1017/S00167568190006451](https://doi.org/10.1017/S00167568190006451).
- Malinovsky AI, Golozoubov VV, Simanenkov VP and Simanenkov LF** (2008) Kema terrane: a fragment of a back-arc basin of the early Cretaceous Moneron–Samarga island-arc system, East Sikhote–Alin range, Russian Far East. *Island Arc* **17**, 285–304. doi: [10.1111/j.1440-1738.2008.00619.x](https://doi.org/10.1111/j.1440-1738.2008.00619.x).
- Maruyama S, Isozaki Y, Kimura G and Terabayashi M** (1997) Paleogeographic maps of the Japanese Islands: plate tectonic synthesis from 750Ma to the present. *Island Arc* **6**, 121–42.
- Meng QR and Zhang GW** (1999) Timing of collision of the North and South China blocks: controversy and reconciliation. *Geology* **27**, 123–6.
- Mooney W and Kaban MK** (2010) The North American upper mantle: density, composition, and evolution. *Journal of Geophysical Research – Solid Earth* **115**, B12424. doi: [10.1029/2010JB008066](https://doi.org/10.1029/2010JB008066).
- Müller RD, Seton M, Zahirovic S, Williams SE, Matthews KJ, Wright NM, Shephard GE, Maloney KT, Barnett-Moore N, Hosseinpour M, Bower DJ and Cannon J** (2016) Ocean basin evolution and global-scale plate reorganization events since Pangea breakup. *Annual Review of Earth and Planetary Sciences* **44**, 107–38.
- Ni JL, Liu JL, Tang XL, Yang H, Xia ZM and Guo QJ** (2013) The Wulian metamorphic core complex: a newly discovered metamorphic core complex along the Sulu Orogenic Belt, Eastern China. *Journal of Earth Science* **24**, 297–313.
- Pang CJ, Krapež B, Li ZX, Xu YG, Liu HQ and Cao J** (2014) Stratigraphic evolution of a Late Triassic to Early Jurassic intracontinental basin in southeastern South China: a consequence of flat-slab subduction? *Sedimentary Geology* **302**, 44–63.
- Pearce JA** (1982) Trace element characteristics of lavas from destructive plate boundaries. In *Orogenic Andesites and Related Rocks*, vol. 8 (ed. RS Thorpe), pp. 525–48. New York: John Wiley and Sons.
- Pearce JA** (1983) Role of the sub-continental lithosphere in magma genesis at active continental margins. In *Continental Basalts and Mantle Xenoliths* (eds CJ Hawkesworth and MJ Norry), pp. 230–49. Cambridge, Massachusetts: Shiva Publishing Ltd.
- Pedoja K, Shen JW, Kershaw S and Tang C** (2008) Coastal Quaternary morphologies on the northern coast of the South China Sea, China, and their implications for current tectonic models: a review and preliminary study. *Marine Geology* **255**, 103–17. doi: [10.1016/j.margeo.2008.02.002](https://doi.org/10.1016/j.margeo.2008.02.002).
- Proffett JM** (1977) Cenozoic geology of the Yerington district, Nevada, and implications for the nature and origin of Basin and Range faulting. *Geological Society of America Bulletin* **88**, 247–66.
- Qi Y, Hu R, Liu S, Coulson IM, Qi H, Tian J, Feng C and Wang T** (2012) Geochemical and Sr–Nd–Pb isotopic compositions of Mesozoic mafic dikes from the Gan–Hang tectonic belt, South China: petrogenesis and geodynamic significance. *International Geology* **54**, 920–39. doi: [10.1080/00206814.2011.588820](https://doi.org/10.1080/00206814.2011.588820).
- Qiu JS, Wang D and Zhou JC** (1999) Geochemistry and petrogenesis of the late Mesozoic bimodal volcanic rocks at Yunshan caldera, Yongtai County, Fujian Province. *Acta Petrologica et Mineralogica* **18**, 97–107 (in Chinese).
- Qiu L, Yan DP, Yang WX, Wang JB, Tang XL and Ariser S** (2017) Early to Middle Triassic sedimentary records in the Youjiang Basin, South China: implications for Indosinian orogenesis. *Journal of Asian Earth Sciences* **141**, 125–39.
- Quelhas P, Mata J and Dias ÁA** (2020) Evidence for mixed contribution of mantle and lower and upper crust to the genesis of Jurassic I-type granites from Macao, SE China. *Geological Society of America Bulletin*, doi: [10.1130/B35552.1](https://doi.org/10.1130/B35552.1).
- Rosenbaum G, Gasparon M, Lucente FP, Peccerillo A and Miller MS** (2008) Kinematics of slab tear faults during subduction segmentation and implications for Italian magmatism. *Tectonics* **27**, TC2008. doi: [10.1029/2007TC002143](https://doi.org/10.1029/2007TC002143).
- Schellart WP** (2020) Control of subduction zone age and size on flat slab subduction. *Frontiers in Earth Science* **8**, 26. doi: [10.3389/feart.2020.00026v](https://doi.org/10.3389/feart.2020.00026v).
- Schellart WP, Freeman J, Stegman DR, Moresi L and May D** (2007) Evolution and diversity of subduction zones controlled by slab width. *Nature* **446**, 308–11. doi: [10.1038/nature05615](https://doi.org/10.1038/nature05615).
- Schellart WP, Stegman DR, Farrington RJ, Freeman J and Moresi L** (2010) Cenozoic tectonics of western North America controlled by evolving width of Farallon slab. *Science* **329**, 316–19.
- Schmandt B and Lin FC** (2014) P and S wave tomography of the mantle beneath the United States. *Geophysical Research Letters* **41**, 6342–49. doi: [10.1002/2014GL061231](https://doi.org/10.1002/2014GL061231).
- Sewell RJ, Tang DLK and Campbell SDG** (2012) Volcanic-plutonic connections in a tilted nested caldera complex in Hong Kong. *Geochemistry, Geophysics, Geosystems* **13**, Q01006. doi: [10.1029/2011GC003865](https://doi.org/10.1029/2011GC003865).
- Shen L, Yu JH, O'Reilly SY and Griffin WL** (2018) Tectonic switching of southeast China in the Late Paleozoic. *Journal of Geophysical Research – Solid Earth* **123**, 8508–26.
- Shu LS, Jahn BM, Charvet J, Santosh M, Wang B, Xu XS and Jiang SY** (2014) Intraplate tectono-magmatism in the Cathaysia Block (South China): evidence from stratigraphic, structural, geochemical and geochronological investigations. *American Journal of Science* **314**, 154–86.
- Shu LS, Wang B, Cawood PA, Santosh M and Xu ZQ** (2015) Early Paleozoic and Early Mesozoic intraplate tectonic and magmatic events in the Cathaysia Block, South China. *Tectonics* **34**, 1600–21. doi: [10.1002/2015TC003835](https://doi.org/10.1002/2015TC003835).
- Shu LS, Wang Y, Sha JG, Jiang SY, Yu JH and Wang YB** (2009) Jurassic sedimentary features and tectonic settings of southeastern China. *Science in China Series D: Earth Sciences* **52**, 1969–78. doi: [10.1007/s11430-009-0159-z](https://doi.org/10.1007/s11430-009-0159-z).
- Stern RJ and Gerya T** (2018) Subduction initiation in nature and models: a review. *Tectonophysics* **746**, 173–98. doi: [10.1016/j.tecto.2017.10.014](https://doi.org/10.1016/j.tecto.2017.10.014).
- Stern RJ, Li SM and Keller GR** (2018) Continental crust of China: a brief guide for the perplexed. *Earth-Science Reviews* **179**, 72–94. doi: [10.1016/j.earscirev.2018.01.020](https://doi.org/10.1016/j.earscirev.2018.01.020).
- Sun M, Chen H, Milan LA, Wilde SA, Jourdan F, and Xu Y** (2018) Continental arc and back-arc migration in eastern NE China: new constraints on Cretaceous Paleo-Pacific subduction and rollback. *Tectonics* **37**, 3893–3915. doi: [10.1029/2018TC005170](https://doi.org/10.1029/2018TC005170).
- Sun MD, Xu YG, Wilde S, Chen HL and Yang SF** (2015) The Permian Dongfanghong island-arc gabbro of the Wandashan Orogen, NE China: implications for Paleo-Pacific subduction. *Tectonophysics* **30**, 122–36.
- Sun WD, Ding X, Hu YH and Li XH** (2007) The golden transformation of the Cretaceous plate subduction in the west Pacific. *Earth and Planetary Science Letters* **262**, 533–42.
- Tang J, Xu WL, Wang F and Ge WC** (2018) Subduction history of the Paleo-Pacific slab beneath Eurasian continent: Mesozoic–Paleogene magmatic records in Northeast Asia. *Science China – Earth Sciences* **61**, 527–59.
- Tang L, Chen H, Dong CW, Yang SF, Shen ZY, Cheng XG and Fu LL** (2013) Middle Triassic post-orogenic extension on Hainan Island: chronology and geochemistry constraints of bimodal intrusive rocks. *Science China – Earth Sciences* **56**, 783–93.
- Tao L, Pan FB, Liu R, Jin C, Jia BJ and He X** (2020) Petrogenesis of the Cretaceous granitoids in Zhejiang, northeast South China Block and their

- implications for episodic retreat and roll-back of the Paleo-Pacific Plate. *Geological Society of America Bulletin*. doi: [10.1130/B35426.1](https://doi.org/10.1130/B35426.1).
- Tao N, Li ZX, Danisik M, Evans NJ, Li RX, Pang CJ, Li WX, Jourdan F, Yu Q, Liu LP, Batt GE and Xu YG (2019) Post-250 Ma thermal evolution of the central Cathaysia Block (SE China) in response to flat-slab subduction at the proto-Western Pacific margin. *Gondwana Research* 75, 1–15.
- Taylor WJ, Bartley JM, Martin MW, Geissman JW, Walker JD, Armstrong PA and Fryxell JE (2000) Relations between hinterland and foreland shortening: Sevier orogeny, central North America Cordillera. *Tectonophysics* 19, 1124–43.
- Tian ZX, Yan Y, Huang CY, Dilek Y, Yu MM, Liu HQ, Zhang XC and Zhang Y (2020) Fingerprinting subducted oceanic crust and Hainan plume in the melt sources of Cenozoic basalts from the South China Sea region. *Terra Nova*, doi: [10.1111/TER.12486](https://doi.org/10.1111/TER.12486).
- Tian ZY, Han P and Xu KD (1992) The Mesozoic Cenozoic East China Rift System. *Tectonophysics* 208, 341–63.
- Ulmer P (2001) Partial melting in the mantle wedge: the role of H₂O in the genesis of mantle-derived 'arc-related' magmas. *Physics of the Earth and Planetary Interiors* 127, 215–32.
- Van Avendonk HJA, McIntosh KD, Kuo-Chen H, Lavier LL, Okaya DA, Wu FT, Wang CY, Lee CS and Liu CS (2016) A lithospheric profile across northern Taiwan: from arc-continent collision to extension. *Geophysical Journal International* 204, 331–46.
- Vazquez JA and Reid MR (2002) Time scales of magma storage and differentiation of voluminous rhyolites at Yellowstone caldera. *Contributions to Mineralogy and Petrology* 144, 274–85.
- Wakita K, Nakagawa T, Sakata M, Tanaka N and Oyama N (2020) Phanerozoic accretionary history of Japan and the western Pacific margin. *Geological Magazine*, doi: [10.1017/S0016756818000742](https://doi.org/10.1017/S0016756818000742).
- Wang C, Zhao X, Huang ZZ, Xing GF and Wang LX (2018) Early Cretaceous extensional-tectonism-related petrology of the Gan-Hang Belt SE China: Lingshan A-type granite at ca. 130 Ma. *Geological Journal* 53, 2487–506. doi: [10.1002/gj.3083](https://doi.org/10.1002/gj.3083).
- Wang D and Shu LS (2012) Late Mesozoic basin and range tectonics and related magmatism in Southeast China. *Geoscience Frontiers* 3, 109–24.
- Wang DZ, Shu LS, Faure M and Sheng WZ (2001) Mesozoic magmatism and granitic dome in the Wugongshan Massif, Jiangxi province and their genetical relationship to the tectonic events in southeast China. *Tectonophysics* 339, 259–77.
- Wang Q, Li JW, Jian P, Zhao ZH, Xiong XL, Bao ZW, Xu JF, Li CF and Ma JL (2005) Alkaline syenites in eastern Cathaysia (South China): link to Permian–Triassic transtension. *Earth and Planetary Science Letters* 230, 339–54.
- Wang SJ, Li X, Schertl H-P and Feng Q (2019) Petrogenesis of early cretaceous andesite dykes in the Sulu orogenic belt, eastern China. *Mineralogy and Petrology* 113, 77–97.
- Wang Y, Wang YJ, Lia S, Seagrenc E, Zhang Y, Zhang P and Qian X (2020) Exhumation and landscape evolution in eastern South China since the Cretaceous: new insights from fission-track thermochronology. *Journal of Asian Earth Sciences* 191, 104239. doi: [10.1016/j.jseae.2020.104239](https://doi.org/10.1016/j.jseae.2020.104239).
- Wang YJ, Fan WM, Zhang GW and Zhang YH (2013) Phanerozoic tectonics of the South China Block: key observations and controversies. *Gondwana Research* 23, 1273–305.
- Wang YJ, Wu CM, Zhang AM, Fan WM, Zhang YH, Zhang YZ, Peng TP and Yin CQ (2012) Kwangian and Indosinian reworking of the eastern South China Block: constraints on zircon U–Pb geochronology and metamorphism of amphibolite and granulite. *Lithos* 150, 227–42.
- Wei W, Song C, Hou Q, Chen Y, Faure M and Yan Q (2018) The Late Jurassic extensional event in the central part of the South China Block: evidence from the Laoshan'ao shear zone and Xiangdong Tungsten deposit (Hunan, SE China). *International Geology Review* 60, 1644–64.
- Wells ML, Hoisch TD, Cruz-Uribe AM and Vervoort JD (2012) Geodynamics of synconvergent extension and tectonic mode switching: constraints from the Sevier-Laramide orogen. *Tectonics* 31(1), TC1002. doi: [10.1029/2011TC002913](https://doi.org/10.1029/2011TC002913).
- Wernicke B and Snow JK (1998) Cenozoic tectonism in the central Basin and Range: motion of the Sierran–Great Valley Block. *International Geology Review* 40, 403–10.
- Wilde SA, Zhou X, Nemchin AA and Sun M (2003) Mesozoic crust–mantle interaction beneath the North China craton: a consequence of the dispersal of Gondwanaland and accretion of Asia. *Geology* 31, 817–20.
- Wu YM, Guo F, Wang XC, Zhang B, Zhang X, Alemayehu M and Wang GQ (2020) Generation of Late Cretaceous Ji'an basalts through asthenosphere–slab interaction in South China. *Geological Society of America Bulletin*, doi: [10.1130/B35196.1](https://doi.org/10.1130/B35196.1).
- Xiao WJ and He HQ (2005) Early Mesozoic thrust tectonics of the northwest Zhejiang region (Southeast China). *Geological Society of America Bulletin* 117, 945–61.
- Xiao Y, Zhang HF, Su BX, Liang Z, Zhu B and Sakya PA (2019) Subduction-driven heterogeneity of the lithospheric mantle beneath the Cathaysia block, South China. *Journal of Asian Earth Sciences* 186, 104062. doi: [10.1016/j.jseae.2019.104062](https://doi.org/10.1016/j.jseae.2019.104062).
- Xu CH, Zhang L, Shi HS, Brix MB, Huhma H, Chen LH, Zhang MQ and Zhou ZY (2017) Tracing an Early Jurassic magmatic arc from South to East China Seas. *Tectonics* 36, 466–92.
- Xu D, Wang Z, Wu C, Zhou YQ, Shan Q, Hou MZ, Fu YG and Zhang XW (2017) Mesozoic gold mineralization in Hainan Province of South China: genetic types, geological characteristics and geodynamic settings. *Journal of Asian Earth Sciences* 137, 80–108. doi: [10.1016/j.jseae.2016.09.004](https://doi.org/10.1016/j.jseae.2016.09.004).
- Xu X, Tang S and Lin S (2015) Tectonic and sedimentary response of the Huangshan Basin to paleo-Pacific subduction underneath Southeast China. American Geophysical Union, Fall Meeting 2015, San Francisco, California (USA), 2015AGUFM.T31B2883X.
- Xu XB, Zhang YQ, Shu LS and Jia D (2011) La-ICP-MS U–Pb and ⁴⁰Ar/³⁹Ar geochronology of the sheared metamorphic rocks in the Wuyishan: constraints on the timing of Early Paleozoic and Early Mesozoic tectono-thermal events in SE China. *Tectonophysics* 501, 71–86.
- Xu YG, Ma JL, Frey FA, Feigenson MD and Liu JF (2005) Role of lithosphere–asthenosphere interaction in the genesis of Quaternary alkali and tholeiitic basalts from Datong, western North China Craton. *Chemical Geology* 224, 247–71.
- Yan DP, Zhou M-F, Song HL, Wang XW and Malpas J (2003) Origin and tectonic significance of a Mesozoic multi-layer over-thrust system within the Yangtze Block (South China). *Tectonophysics* 361, 239–54.
- Yang L-Q, Dilek Y, Weinburg RF and Liu Y (2018) Late Jurassic, high-Ba-Sr Linglong granites in the Jiaodong Peninsula, East China: lower crustal melting products in the Eastern North China Craton. *Geological Magazine* 155, 1040–62. doi: [10.1017/S0016756816001230](https://doi.org/10.1017/S0016756816001230).
- Yang SX and Yu PR (1994) The characteristics of shallower imbricate nappe structure along Pushi–Chenxi and its significance in searching mineral resources. *Hunan Geology* 14, 31–4 (in Chinese with English abstract).
- Yang SY, Jiang SY, Jiang YH, Zhao K and Fan HH (2011) Geochemical, zircon U–Pb dating and Sr–Nd–Hf isotopic constraints on the age and petrogenesis of an Early Cretaceous volcanic–intrusive complex at Xiangshan, Southeast China. *Mineralogy and Petrology* 101, 21–48. doi: [10.1007/s00710-010-0136-4](https://doi.org/10.1007/s00710-010-0136-4).
- Yang Y-Z, Wang Y, Ye R-S, Li S-Q, He J-F, Siebel W and Chen F (2017) Petrology and geochemistry of Early Cretaceous A-type granitoids and late Mesozoic mafic dikes and their relationship to adakitic intrusions in the lower Yangtze River belt, Southeast China. *International Geology Review* 59, 62–79. doi: [10.1080/00206814.2016.1212284](https://doi.org/10.1080/00206814.2016.1212284).
- Yao W, Li ZX, Li WX and Li XH (2017) Proterozoic tectonics of Hainan Island in supercontinent cycles: new insights from geochronological and isotopic results. *Precambrian Research* 290, 86–100.
- Yi K, Cheong C-s, Kim J, Kim N, Jeong YJ and Cho M (2012) Late Paleozoic to Early Mesozoic arc-related magmatism in southeastern Korea: SHRIMP zircon geochronology and geochemistry. *Lithos* 153, 129–41. doi: [10.1016/j.lithos.2012.02.007](https://doi.org/10.1016/j.lithos.2012.02.007).
- Yiu TF, Chu HT, Suga K, Lan CY, Chung SH, Wang KL and Grove M (2017) Subduction-related 200 Ma Talun metagranite, SE Taiwan: an age constraint for Palaeo-Pacific plate subduction beneath South China Block during the Mesozoic. *International Geology Review* 59, 333–46. doi: [10.1080/00206814.2016.1261259](https://doi.org/10.1080/00206814.2016.1261259).
- Zahirovic S, Seton M and Müller RD (2014) The Cretaceous and Cenozoic tectonic evolution of Southeast Asia. *Solid Earth* 5, 227–73. doi: [10.5194/se-5-227-2014](https://doi.org/10.5194/se-5-227-2014).

- Zhang FQ, Wu HX, Dilek Y, Zhang W, Zhu KY and Chen HL (2020) Guadalupian (Permian) onset of subduction zone volcanism and geodynamic turnover from passive to active margin tectonics in southeast China. *Geological Society of America Bulletin* **132**, 130–48. doi: [10.1130/B32014.1](https://doi.org/10.1130/B32014.1).
- Zhang GW, Guo AL, Wang YJ, Li SZ, Dong YP, Liu SF, He DF, Cheng SY, Lu RK and Yao AP (2013) Tectonics of South China Continent and its implications. *Science China: Earth Sciences* **56**, 1804–28. doi: [10.1007/s11430-013-4679-1](https://doi.org/10.1007/s11430-013-4679-1).
- Zhang K, Lü Q, Zhao JH, Yan JY, Hu H, Luo F, Fu GM and Tao X (2020) Magnetotelluric evidence for the multi-microcontinental composition of eastern South China and its tectonic evolution: nature. *Scientific Reports* **10**, 13105. doi: [10.1038/s41598-020-69777-3](https://doi.org/10.1038/s41598-020-69777-3).
- Zhang KJ and Cai JX (2009) NE–SW-trending Hepu–Hetai dextral shear zone in southern China: penetration of the Yunkai promontory of South China into Indochina. *Journal of Structural Geology* **31**, 737–48.
- Zhang R, Wu Y, Gao Z, Fu YV, Sun L, Wu Q and Ding Z (2017) Upper mantle discontinuity structure beneath eastern and southeastern Tibet: new constraints on the Tengchong intraplate volcano and signatures of detached lithosphere under the western Yangtze Craton. *Journal of Geophysical Research: Solid Earth* **122**, 1367–80. doi: [10.1002/2016JB013551](https://doi.org/10.1002/2016JB013551).
- Zhang W, Wu H-X, Zhu K-Y, Zhang K-F, Xing X-L, Chen D-X, Chen HL and Zhang F-Q (2018) The Jurassic magmatism and its tectonic setting in the eastern margin of South China: evidence from the volcanic rocks of the Maonong Formation in the SE Zhejiang. *Acta Geologica Sinica* **34**, 3375–98.
- Zhang X, Takeuchi M, Ohkawa M and Matsuzawa N (2018) Provenance of a Permian accretionary complex (Nishiki Group) of the Akiyoshi Belt in southwest Japan and paleogeographic implications. *Journal of Asian Earth Sciences* **167**, 130–8. doi: [10.1016/j.jseas.2018.01.005](https://doi.org/10.1016/j.jseas.2018.01.005).
- Zhang Y, Dilek Y, Zhang FQ, Chen HL, Zhu CT and Hao XF (2020) Structural architecture and tectonic evolution of the Cenozoic Zhanhua Sag along the Tan–Lu Fault Zone in the eastern North China: reconciliation of tectonic models on the origin of the Bohai Bay Basin. *Tectonophysics* **775**. doi: [10.1016/j.tecto.2019.228303](https://doi.org/10.1016/j.tecto.2019.228303).
- Zhang YF, Wang Y, Zhao Y and Jin Z (2016) On velocity anomalies beneath southeastern China: an investigation combining mineral physics studies and seismic tomography observations. *Gondwana Research* **31**, 200–17.
- Zhang Z and Wang Y (2007) Crustal structure and contact relationship revealed from deep seismic sounding data in South China. *Physics of the Earth and Planetary Interiors* **165**, 114–26. doi: [10.1016/j.pepi.2007.08.005](https://doi.org/10.1016/j.pepi.2007.08.005).
- Zhang Z, Xu T, Zhao B and Badal J (2013) Systematic variations in seismic velocity and reflection in the crust of Cathaysia: new constraints on intraplate orogeny in the South China continent. *Gondwana Research* **24**, 902–17.
- Zhao B, Bai ZM, Xu T, Zhang Z and Badal J (2013) Lithological model of the South China crust based on integrated geophysical data. *Journal of Geophysics and Engineering* **10**. doi: [10.1088/1742-2132/10/2/025005](https://doi.org/10.1088/1742-2132/10/2/025005).
- Zhao L, Zhai MG, Zhou XW, Santosh M and Ma XD (2015) Geochronology and geochemistry of a suite of mafic rocks in Chencai area, South China: implications for petrogenesis and tectonic setting. *Lithos* **236–237**, 226–44. doi: [10.1016/j.lithos.2015.09.004](https://doi.org/10.1016/j.lithos.2015.09.004).
- Zhao X, Yu SY, Jiang Y, Mao J, Yu MG, Chen ZH and Xing GF (2019) Petrogenesis of two stages of Cretaceous granites in southwest Fujian Province: implications for the tectonic transition of South-East China. *Geological Journal* **54**, 221–44.
- Zheng Y, Xu Z, Zhao Z and Dai L (2018) Mesozoic mafic magmatism in North China: implications for thinning and destruction of cratonic lithosphere. *Science China Earth Sciences* **61**, 353–85.
- Zhou JB, Cao J, Wilde SA, Zhao G, Zhang J and Wang B (2014) Paleo-Pacific subduction-accretion: evidence from geochemical and U–Pb zircon dating of the Nanhada accretionary complex, NE China. *Tectonics* **33**, 2444–66.
- Zhou JB and Li L (2017) The Mesozoic accretionary complex in Northeast China: evidence for the accretion history of Paleo-Pacific subduction. *Journal of Asian Earth Sciences* **145**, 91–100.
- Zhou JC and Chen R (2001) Geochemistry of late Mesozoic interaction between crust and mantle in southeastern Fujian Province. *Geochimica* **30**, 547–58. doi: [10.1007/BF02882602](https://doi.org/10.1007/BF02882602).
- Zhou L, Xie J, Shen W, Zheng Y, Yang Y, Shi H and Ritzwoller MH (2012) The structure of the crust and uppermost mantle beneath South China from ambient noise and earthquake tomography. *Geophysical Journal International* **189**, 1565–83. doi: [10.1111/j.1365-246X.2012.05423.x](https://doi.org/10.1111/j.1365-246X.2012.05423.x).
- Zhou XM and Li WX (2000) Origin of Late Mesozoic igneous rocks in southeastern China: implications for lithosphere subduction and underplating of mafic magmas. *Tectonophysics* **326**, 269–87.
- Zhou XM, Sun T, Shen WZ, Shu LS and Niu Y (2006) Petrogenesis of Mesozoic granitoids and volcanic rocks in South China: a response to tectonic evolution. *Episodes* **29**, 26–33.
- Zhou Y, Liang XQ, Kröner A, Cai YF, Shao T, Wen S, Jiang Y, Fu J, Wang C and Dong C (2015) Late Cretaceous lithospheric extension in SE China: constraints from volcanic rocks in Hainan Island. *Lithos* **232**, 100–10. doi: [10.1016/j.lithos.2015.06.028](https://doi.org/10.1016/j.lithos.2015.06.028).
- Zhu KY, Li ZX, Xia QK, Xu XS, Wilde SA and Chen HL (2017) Revisiting Mesozoic felsic intrusions in eastern South China: spatial and temporal variations and tectonic significance. *Lithos* **294–295**, 147–63.
- Zhu KY, Li ZX, Xu XS and Wilde SA (2013) Late Triassic melting of a thickened crust in southeastern China: evidence for flat-slab subduction of the Paleo-Pacific plate. *Journal of Asian Earth Sciences* **74**, 265–79.
- Zhu KY, Li ZX, Xu XS and Wilde SA (2014) A Mesozoic Andean – type orogenic cycle in southeastern China as recorded by granitoid evolution. *American Journal of Science* **314**, 187–234.
- Zindler A and Hart SR (1986) Chemical geodynamics. *Annual Review of Earth and Planetary Sciences* **14**, 493–571. doi: [10.1146/annurev.ea.14.050186.002425](https://doi.org/10.1146/annurev.ea.14.050186.002425).